This is a repository copy of *Hydroclimate variability was the main control on fire activity in northern Africa over the last 50,000 years*.

Hydroclimate variability was the main control on fire activity in northern Africa over the last 50,000 years

Harriet R. Moore [a], [1], Anya J. Crocker [a], [b], [*], [1], Claire M. Belcher [c], A. Nele Meckler [d], Colin P. Osborne [b], David J. Beerling [b], Paul A. Wilson [a]

[a] University of Southampton, Waterfront Campus, National Oceanography Centre Southampton, SO14 3ZH, United Kingdom
[b] Department of Animal and Plant Sciences, University of Sheffield, Sheffield, S10 2TN, United Kingdom
[c] wildFIRE Lab, University of Exeter, Exeter, EX4 4PS, United Kingdom
[d] Bjerknes Centre for Climate Research and Department of Earth Science, University of Bergen, 5007, Bergen, Norway

ARTICLE INFO

ABSTRACT

North Africa features some of the most frequently burnt biomes on Earth, including the semi-arid grasslands of the Sahel and wetter savannas immediately to the south. Natural fires are fuelled by rapid biomass production during the wet season, its desiccation during the dry season and ignition by frequent dry lightning strikes. Today, fire activity decreases markedly both to the north of the Sahel, where rainfall is extremely low, almost eliminating biomass over the Sahara, and to the south where forest biomes are too wet to burn. Over the last glacial cycle, rainfall and vegetation cover over northern Africa varied dramatically in response to gradual astronomically-forced insolation change, changes in atmospheric carbon dioxide levels, and abrupt cooling events over the North Atlantic Ocean associated with the reorganisation of Meridional Overturning Circulation (MOC). Here we report the results of a study into the impact of these climate changes on fire activity in northern African over the last 50,000 years (50 kyr). Our reconstructions come from marine sediments with strong age control that provide an uninterrupted record of charcoal particles exported from the African continent. We studied three sites on a latitudinal transect along the northwest African margin between 21 and 9°N. Our sites exhibit a distinct latitudinal relationship between past changes in rainfall and fire activity. At the southernmost site (GeoB9528-3, 9°N), fire activity decreased during intervals of increasing humidity, while our northern-most site (ODP Site 658, 21°N) clearly demonstrates the opposite relationship. The site in the middle of our transect, offshore of the present day southern Sahel today (GeoB9508-5, 15°N), exhibits a "Goldi-locks" relationship between fire activity and hydroclimate, wherein charcoal fluxes peak under inter-mediate rainfall climate conditions and are supressed by transition to more arid or more humid conditions. Our results are remarkably consistent with the predictions of the intermediate fire-productivity hypothesis developed in conceptual macroecological models and supported by empirical evidence of modern day fire activity. Feedback processes operating between fire, climate and vegetation are undoubtedly complex but temperature is suggested to be the main driver of temporal change in fire activity globally, with the precipitation-evaporation balance perhaps a secondary influence in the Ho-locene tropics. However, there is only sparse coverage of Africa in the composite records upon which those interpretations are based. We conclude that hydroclimate (not temperature) exerted the dominant control on burning in the tropics of northern Africa well before the Holocene (from at least 50 ka).

1. Introduction

Fire has long been recognized as a major driver of ecological change over both observational and geological time scales. It plays a role in both the global carbon cycle and the release and redistribution of nutrients (Archibald et al., 2018). In savannas, fires control the structure of ecosystems by favouring flammable grasses and

* Corresponding author. University of Southampton, Waterfront Campus, National Oceanography Centre Southampton, SO14 3ZH, United Kingdom.
  E-mail address: anya.crocker@noc.soton.ac.uk (A.J. Crocker).
[1] These authors contributed equally to this work.

grazing herbivores over trees and browsing herbivores (Archibald and Hempson, 2016). Consequently, fire is largely responsible for the maintenance of wetter savanna biomes, which would transition into forest without regular disturbance (Accatino et al., 2010; Beckage et al., 2009; Bond et al., 2005; Sankaran et al., 2005; Staver et al., 2011b). Fires also shape ecosystems over geological time-scales, for example, by acting as a positive feedback on the expansion of the C$_4$ savanna ecosystem since the Late Miocene (Beerling and Osborne, 2006; Bond et al., 2003; Hoetzel et al., 2013; Keeley and Rundel, 2005; Osborne and Beerling, 2006).

Ecosystem flammability is determined by a complex interplay of climatological and ecological factors that influence the amount of biomass available to burn (i.e. fuel load) and its moisture content (i.e. ignitability and spreadability) (Pausas et al., 2017; Simpson et al., 2016). Natural fires in the Sahel are fuelled by rapid biomass production during the wet season, its desiccation during the dry season and ignition by frequent dry lightning strikes. The rapid regenerative capacity and high water- and nitrogen-use efficiencies of grasses, which typically use the C$_4$ photosynthetic pathway in low latitude savannas, allow the generation of copious highly flammable fuels that desiccate during the dry season (Ripley et al., 2010). Woody plants in savannas (commonly C$_3$) typically have inflammable characteristics such as thick, fire-retardant bark and produce smaller fuel loads with a higher moisture content (Pausas et al., 2017). The balance between grassy and woody plants is strongly affected by the amount and seasonality of precipitation, which also has a direct influence on the flammability of the biomass produced (D'Onofrio et al., 2018; Pausas and Ribeiro, 2013). Increased precipitation generally leads to a greater fuel load. However, if precipitation levels are too high, periods of dry weather are not long or regular enough to allow the fuel to properly dry out, ignition and fire spread are limited by fuel moisture, and tree growth may be promoted at the expense of grasslands (Sankaran et al., 2005; Staver et al., 2011b).

Modern fire activity in northern Africa exhibits a very strong sensitivity to precipitation (Fig. 1). Natural fires in the region peak around ~15 to 9°N, where biomass production over high-rainfall, broad-leaf savanna grasslands responds quickly to the wet season, generating large fuel stocks which are desiccated during the dry season and ignited by frequent dry lightning strikes (Archibald and Hempson, 2016). Fire activities decrease to the south where mean annual precipitation (MAP) is higher (>1000 mm/yr), suppressing fire activity by promoting the growth of more fire-resistant vegetation and/or reducing the desiccation of biomass, with increased tree cover in woodlands and mosaics of forest shading and suppressing the growth of flammable grasses (Giglio et al., 2006; Sankaran et al., 2005; van der Werf et al., 2006; White, 1983). The modern threshold for fire suppression occurs at ca. 40% woody cover, above which high tree canopy covers exclude fuel-producing grasses (particularly the most flammable), resulting in small, high moisture-content fuel loads (Archibald et al., 2009; Cardoso et al., 2018; Hoffmann et al., 2012; Sankaran et al., 2005; Staver et al., 2011a). Fire activities also decrease to the north of about 15°N, where MAP is lower (<500 mm/yr) and climatically maintained dry savannas transition into semi-desert and desert where fuel accumulation is insufficient to support frequent fires, vegetation is often discontinuous limiting fire spread, and the absence of trees reduces ignition frequency (Fig. 1) (e.g. Archibald and Hempson, 2016; Giglio et al., 2006). Thus, the fire activity map of northern Africa is strikingly closely related to rainfall distribution in the region, showing a 'humped' relationship with MAP, biomass and therefore latitude, with peak fire activities occurring with mean annual precipitation values of about 800–1400 mm/yr (Archibald and Hempson, 2016; van der Werf et al., 2008 and Fig. 2).

This relationship between fire, precipitation and productivity

observed in Africa today is encapsulated by the intermediate fire-productivity hypothesis, developed in conceptual macroecological models and supported by empirical evidence of modern day fire activity (e.g. Archibald and Hempson, 2016; Bowman et al., 2014; Clarke et al., 2020; Krawchuk et al., 2009; Pausas and Ribeiro, 2013; Whitlock et al., 2010). While these models provide an excellent description of present day fire-climate relationships, using them to predict changes in fire activity through time is not straightforward because they do not explicitly incorporate the complex feedbacks between climate, vegetation and fire that underpin the fire-productivity relationship (Bowman et al., 2014; Clarke et al., 2020). Also, ecosystems of the past (and future) may not be directly analogous to those of today, at least in part due to human activities (e.g. Archibald, 2016; Hély et al., 2014; Watrin et al., 2009; Whitlock et al., 2010). Therefore, we turn to palaeo records to better understand how vegetation and fire respond to changes in climate. Analysis of composite sedimentary records from the Global Palaeofire Working Group (GPWG) Global Charcoal Database suggests that temperature was quantitatively the most important predictor of global biomass burning over the last 21 kyrs with the precipitation-evaporation balance a secondary factor, for example, in the northern subtropics during the Holocene (Daniau et al., 2012). Yet Africa, which is home to one of the most frequently burned biomes on Earth today and experienced major changes in rainfall during the recent geological past (e.g. deMenocal, 1995; Mulitza et al., 2008b; Tiedemann et al., 1994; Tierney et al., 2017), is poorly represented in these composite records, particularly north of the equator.

Today, rainfall and the precipitation-evaporation balance in northern Africa are strongly seasonal, with regional jet systems influencing the annual migrations of the tropical rainbelt, roughly paralleling the Intertropical Convergence Zone (ITCZ) low pressure zone which tracks northwards during the boreal summer and moves equatorwards during the boreal winter (Nicholson, 2009; Nicholson and Grist, 2003). On centennial to astronomical time-scales, however, the latitudinal limits of these migrations and geographical extent of the rainbelt have changed, with major consequences for African vegetation (e.g. Collins et al., 2013a; Collins et al., 2011; Dupont, 1993; Larrasoaña et al., 2013).

Over the last 50 kyrs, Earth's climate underwent marked temporal change in insolation forcing, atmospheric CO$_2$ levels, temperature and land ice volume. On Africa, perhaps the most prominent biotic impacts were driven by hydroclimate change and these carried a strong latitudinal imprint (Dupont, 2011). Increases in boreal summer insolation at low latitudes driven by variability in Earth's orbit of the Sun, particularly the precession of the equinoxes on an approximately 20 kyr timescale (with insolation maxima during precession minima), induced more pronounced seasonal ITCZ migration to higher latitudes bringing increased rainfall to much of northern Africa (e.g. Larrasoaña et al., 2013; Prell and Kutzbach, 1987). These intervals are known as African Humid Periods (AHPs) and are exemplified by a large-scale greening of the Saharan Desert (Hély et al., 2014; Ritchie et al., 1985; Claussen et al., 2017). In contrast, widespread cooling of sea surface temperatures in the North Atlantic Ocean associated with abundant iceberg calving and the related influx of freshwater to the ocean at high northern latitudes during the Heinrich (H-) events of the Last Glacial Period resulted in a marked southward displacement of the ITCZ over northern Africa and a >1000 km shift of the boundary between the Saharan Desert and the Sahel towards the equator (Collins et al., 2013a; Mulitza et al., 2008b).

Here we report the results of a study of the fire activity response to these pronounced changes in northern African rainfall climate over the past 50 kyr. We present reconstructions of charcoal accumulation for three marine sediment cores at sites located on a
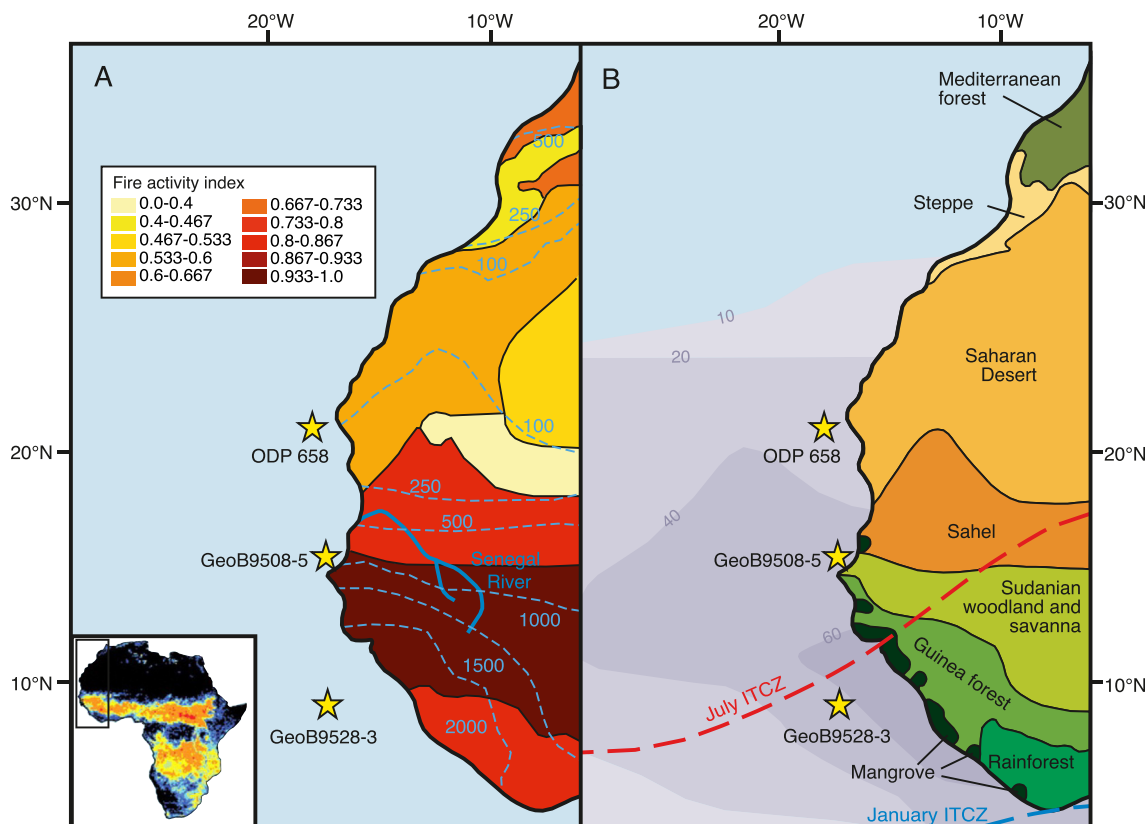
Fig. 1. Our latitudinal transect of study sites: ODP 658 (21°N), GeoB9508-5 (15°N) and GeoB9528-3 (9°N). (A) Fire Activity Index, indicating the average number of fire incidents per unit area, rescaled onto a global scale of 0−1 (redrawn from Pausas and Ribeiro, 2013) and present day mean annual precipitation contours (from Larrasoaña et al., 2013). Inset shows study area marked onto pan-African annual average number of fires estimated by MODIS, with hot colours indicating the highest fire incidences (image from Bowman et al., 2009; data from Giglio et al., 2006) with area covered in the main figure indicated. (B) Schematic showing the major North African vegetation bands (adapted from Hooghiemstra and Agwu, 1986; Kuechler et al., 2013) with the modern mean summer and winter latitudinal position of the ITCZ (Yan, 2005). Purple shading indicates 2007−2016 average annual dust fluxes (in mm m^{-2} day^{-1}) estimated using Infrared Atmospheric Sounding Interferometer (Yu et al., 2019). (For interpretation of the references to colour in this figure legend, the reader is referred to the Web version of this article.)
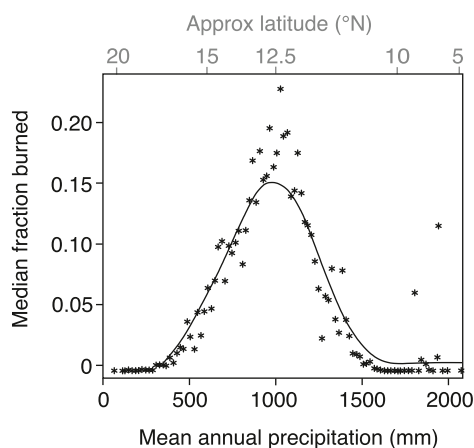
Fig. 2. The relationship between mean annual precipitation and the fraction of land area burned in modern sub-Saharan Africa. Redrawn from Archibald and Hempson (2016), with approximate latitudes corresponding to the precipitation values today along the 10°W meridian indicated on the top axis. Data points represent the median value per 50 mm rainfall band with a loess regression fitted (solid line).

latitudinal transect along the northwest African margin. We exploit marine archives because of their proven potential to yield continuous, largely undisturbed, sequences of exported terrestrial material with excellent age control, allowing us to examine long,

regionally integrated reconstructions of past fire activity on land (e.g. Bird and Cali, 1998; Daniau et al., 2013; Dupont and Schefuß, 2018; Herring, 1985; Hoetzel et al., 2013; Verardo and Ruddiman, 1996).

2. Materials and methods

2.1. Site locations

We studied marine sediments from three sites offshore of northwestern Africa which form a latitudinal transect spanning the modern biome transitions from desert, through savanna, into semi-deciduous forest (Table 1, Fig. 1). All three sites receive windblown terrigenous material from the African continent due to the influence of the African Easterly Jet (AEJ) and northeasterly trade winds, including microscopic charcoal (<1 mm), which is lofted into the air by thermal buoyancy generated during fires (Clark, 1988). South of 17°N, the Senegal and Gambia rivers drain into the Atlantic Ocean from the African continent depositing terrigenous material onto the continental margin, with evidence of river activity further north during past humid periods (Drake et al., 2011; Krastel et al., 2004; Skonieczny et al., 2015).

2.2. Charcoal counts

Herein we define charcoal as any carbon-rich terrestrially derived material produced by combustion triggered by either

Table 1
List of marine sediment cores sampled for charcoal in this study.

Site Name	Latitude (°N)	Longitude (°W)	Water depth (m)	Reference for age model(s) used
ODP Site 658 (ODP 658)	20°44.95′	18°34.85′	2263	Meckler et al. (2013)
GeoB9508-5 (GB-08)	15°29.90′	17°56.88′	2384	Waelbroeck et al. (2019) and Mulitza et al. (2008b)
GeoB9528-3 (GB-28)	9°9.99′	17°39.81′	3057	Schreuder et al. (2019)

natural (lightning strikes) or anthropogenic processes. Charcoal accumulation rates are used to infer fire activity (larger charcoal fluxes indicate increased fire activity), and have also been proven to correlate with burned area in certain environments (e.g. Higuera et al., 2011). Transport and preservation are not inferred to exert a major control on charcoal fluxes to our sites (see section 3.1).

Slides for charcoal counts were prepared following a modified palynological method for marine sediments (based upon Eldrett et al., 2004). Approximately 2−5 g of oven dried bulk sediment was treated with HCl and HF to remove carbonate and silicate material respectively. A combination of boiling HCl, ultrasonic treatment and sieving at 15 μ m was used to remove fluoride compounds and amorphous organic material (AOM) from the samples and each sample was then spiked with a known dose of exotic *Lycopodium* spores (Stockmarr, 1971). We tested whether ultrasonification could lead to fragmentation of charcoal particles using a batch of 15 pilot samples and found no effect, hence we used this step to aid removal of AOM and fluoride compounds.

Mounts of the >15 μ m fraction were examined under trans-

Fluxes were estimated using the sedimentation rates calculated from the age model for each site, following equation (2). Dry bulk densities at Site 658 are calculated from gamma-ray attenuation bulk density measurements (Ruddiman et al., 1989), while sediment density is derived from electrical resistivity measurements at GB-08 (Mulitza et al., 2008a), with sediment water content corrected for at both sites. At GB-28, sediment dry bulk densities are from Schreuder et al. (2019). Flux estimates based on sedimentation rates can be influenced by rapid changes in depositional flux (due to processes such as carbonate dissolution, sediment focussing/winnowing etc.) that occur between age tie-points. However, comparison with flux estimates calculated from $^{230}Th_{xs}$ measurements at ODP 658 (Adkins et al., 2006; Kinsley et al., 2022) indicates that unresolved sedimetation rate fluctuations are not a major control on our charcoal flux reconstructions at this site (see Supplementary Information).

$$Charcoal\ flux\ \left(cm^{-2}\ kyr^{-1}\right) = \left[Charcoal\ concentration\ \left(g^{-1}\right)\right] \times \left[Sedimentation\ rate\ \left(cm\ kyr^{-1}\right)\right] \times \left[Dry\ bulk\ density\ \left(g\ cm^{-3}\right)\right]$$

(2)

mitted light. Optical charcoal identification was achieved using an Olympus BH-2 microscope in conjunction with a freestanding lamp, using the shape, colour and reflectance characteristics of particles. For a particle to be classified as charcoal, it was required to be completely black and fit into one of the following morphological categories; elongate, splintery perforated, splintery unperforated, irregular perforated or square/rectangular. High top light and low bottom light was used to separate charcoal particles from pyrite on the basis of reflectance level; non- or faintly reflectively particles were classified as charcoal whilst highly reflectively particles were classified as pyrite. A selection of representative images of charcoal particles from Site 658 are shown in Fig. 3.

Concurrent counting of charcoal particles and *Lycopodium* spores continued until 500 spores were reached. The ratio of charcoal particles to *Lycopodium* spores in the counted fraction was used to calculate bulk sediment charcoal concentrations, following equation (1). Repeat tests on reprocessed and recounted samples show that our charcoal concentration values have a mean error of ca. ±7%.

2.3. Total organic carbon (% TOC)

A 1 g split of bulk sediment was freeze-dried, ground to fine powder using an agate pestle and mortar and decarbonated overnight in 10% HCl to remove inorganic carbon (in the form of carbonate). The decarbonated residue was then neutralised, oven dried at 50 °C, homogenized and re-weighed to calculate the mass loss of inorganic carbon in the form of carbonate. Approximately 10 mg of dried, decarbonated residue was weighed and sealed into tin capsules for analysis of nitrogen (%N) and organic carbon contents (%C$_{org}$) using an Elementar Vario Isotope Select Elemental Analyser at the University of Southampton's Waterfront Campus. These data were calibrated using standards of L-glutamic acid and peat soil (standard deviation values of 0.19% and 0.16%, respectively). The percentage Total Organic Carbon (%TOC) in bulk sediment was then calculated by adjusting for the mass lost during decarbonation.

$$Charcoal\ concentration\ \left(g^{-1}\right) = \frac{\left[\frac{Counted\ charcoal}{Counted\ \text{Lycopodium}\ spores}\right] \times total\ \text{Lycopodium}\ spores\ added}{Dry\ sediment\ mass\ (g)}$$

(1)
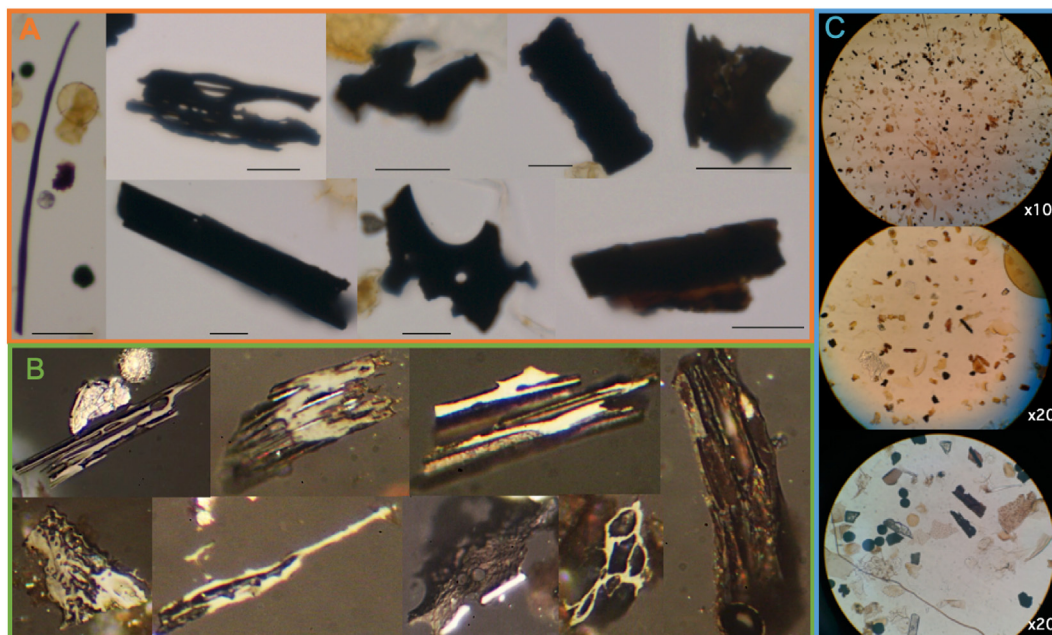
Fig. 3. Representative charcoal particles from ODP Site 658. A) Charcoal particles viewed in transmitted light, with the black scale bar indicating 20 μm. B) Charcoal particles viewed in reflected light. C) Typical views of the processed samples in reflected light, with magnifications stated in the bottom right corners.

2.4. Stratigraphy

Data from ODP 658 are presented on the age model of Meckler et al. (2013), which was produced by first tuning $\delta^{18}O_{benthic}$ data from ODP 658 on a composite depth scale to the LR04 stack (Lisiecki and Raymo, 2005) using the AnalySeries software package (Paillard et al., 1996). Ages were refined by matching XRF-derived Ca from Hole 658A to %CaCO$_3$ in radiocarbon-dated Hole 658C (deMenocal et al., 2000) and tuning ln[Zr/Al] data (a proxy for grain size) from ODP 658 to the grain size-based humidity index from nearby core GeoB7920-2 (Meckler et al., 2013; Tjallingii et al., 2008). Published data from 658C are plotted on the age model of Kinsley et al. (2022).

GB-08 data are plotted on the age model of Waelbroeck et al. (2019), which is based on recalibration of radiocarbon dates of mixed planktonic foraminifera with an age-depth modelling routine accounting for uncertainties in both age and depth. Additional age constraint in the oldest part of the record is provided by correlation of benthic oxygen isotope data from GB-08 to the record from Iberian Margin site MD95-2042 (Mulitza et al., 2008b; Shackleton et al., 2004).

Data from site GB-28 are plotted on the age model of Schreuder et al. (2019), which is based on correlation of benthic oxygen isotope data to the deep North Atlantic and global benthic oxygen stacks (Lisiecki and Raymo, 2005; Lisiecki and Stern, 2016), with down core uncertainty modelled using the R script BACON (Blaauw and Christen, 2011).

3. Results and discussion

3.1. Charcoal transport and preservation

The flux of charcoal calculated from preserved fragments in marine sediments does not simply record the rate of charcoal production on the nearby continent. Instead, the efficiency by which particles are transported to our sites and the degree to which charcoal particles are preserved both have the potential to influence charcoal concentrations in sediment. Here we consider the degree to which these processes may have influenced the charcoal fluxes presented in this study.

3.1.1. Preservation

Charcoal is widely considered to be highly refractory and resistant to degradation (e.g. Goldberg, 1985). Yet, multiple studies suggest that large amounts of charcoal and other forms of black carbon may be oxidised under the correct conditions (e.g. Bird et al., 1999; Masiello, 2004). Most organic matter found in marine sediments is much less refractory than charcoal, therefore TOC values close to zero are required for charcoal to be removed from marine sediments by oxidation. We find no statistically significant relationship between the concentrations of organic carbon and charcoal at ODP 658 (Pearson's correlation co-efficient = 0.15, p-value = 0.475, in agreement with the results of robust regression analysis which shows that it is not possible to conclusively identify either positive or negative correlation between the two variables, Fig. 4). This result suggests that preservation is not a major influence on charcoal flux variability. We therefore find that the observed changes in charcoal flux accurately represent charcoal accumulation in the sediments.

3.1.2. Transport

Charcoal and lithogenic material can be transported from the continents to marine sediments either by rivers or by wind, and can be transported within the ocean by currents. Grain-size based reconstructions suggest that the lithogenic component of marine sediments very close to ODP 658 varies from ~90% aeolian to ~90% riverine origin during the last 50 kyr (Tjallingii et al., 2008), and geochemistry-based estimates of the proportion of dust in lithogenic material are 1−88% and 1−30% at GB-08 and GB-28 respectively (Collins et al., 2013a). If either winds or rivers were much more effective at transporting charcoal than the other, changes in the proportion of riverine and aeolian material deposited offshore would create variability in charcoal fluxes recorded at our sites, even if fire activity remained constant. Yet, while the highest charcoal fluxes to ODP 658 are generally recorded during wet

periods (Fig. 5) when river discharge has been documented from geologically ephemeral rivers on the North West African Margin (Drake et al., 2011; Skonieczny et al., 2015; Tjallingii et al., 2008), the relationship between hydroclimate and charcoal flux is very different at the other two sites further south, where climate is more humid and river systems are more extensive (Figs. 6 and 7). These contrasting site-to-site relationships between charcoal accumulation rates and changes in rainfall climate over the last 50 kyr show that any differences in efficiency of transport by rivers and winds are not a main factor driving charcoal variability at our sites.

Another factor to consider is changes in wind strength (particularly gustiness) (McGee et al., 2013; Tiedemann et al., 1994). There have been major fluctuations in wind strength through the last 50 kyr (McGee et al., 2013; Skonieczny et al., 2019) which impact the capacity of wind to transport charcoal particles offshore, although the position of the African Easterly Jet is suggested to have remained broadly stable (Grousset et al., 1998; Hooghiemstra et al., 2006). Yet a transect of records of dust export along the NW African margin broadly show the same trends through the last 20 kyr with highest fluxes during Heinrich Stadial 1 and the Younger Dryas and lowest fluxes during African Humid Period 1 (McGee et al., 2013). Therefore, because we record very different temporal variability in charcoal flux at our three sites, we conclude that changes in wind strength are not the main factor driving charcoal variability. This conclusion is emphasised by the different relationship between charcoal and dust accumulation at each site (see section 3.2).

3.2. Variability in northern African fire activity over the past 50 kyr

Our records of charcoal flux along the northwest African margin at 21°N (ODP 658), 15°N (GB-08) and 9°N (GB-28) reveal strong latitudinal variability in fire activity in response to both astronomically paced and millennial-scale climatic events over the last 50 kyrs. In Figs. 5–7, we compare our records to reconstructions of hydroclimate and dust fluxes to better understand the relationship between climate and fire activity.
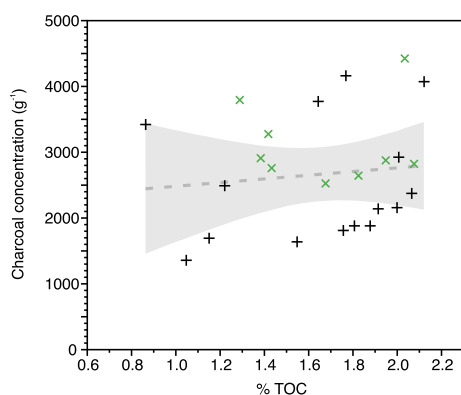
3.2.1. The Last Glacial Maximum and Holocene

The climate of the Last Glacial Maximum (LGM, ca. 26.5–19 ka) was marked in Northern Africa by high dust fluxes, attributed to both increased aridity and high wind speeds, reconstructed at all three of our study sites (Figs. 5–7) (Adkins et al., 2006; Collins et al., 2013a; Kinsley et al., 2022; McGee et al., 2013; Straub et al., 2013) and supported by high δD values of plant waxes along the

Fig. 4. Cross plot of charcoal concentration plotted against % total organic carbon (TOC) for ODP 658 samples. Green crosses indicate Holocene samples, black plusses indicate glacial-aged samples. Grey dashed line and shaded area indicate results of robust regression using the Huber weighting function. (For interpretation of the references to colour in this figure legend, the reader is referred to the Web version of this article.)
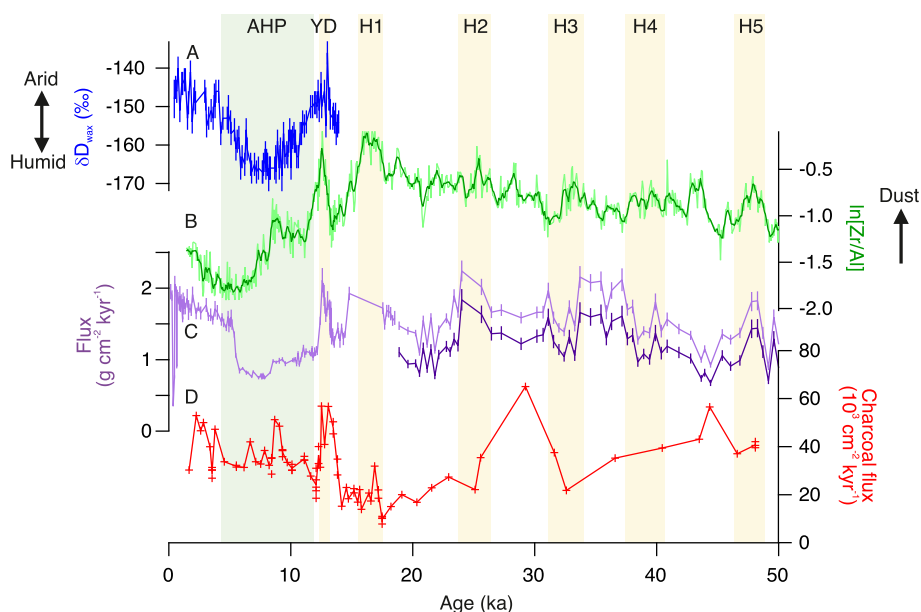
northwest African margin (Niedermeyer et al., 2010; Tierney et al., 2017). In contrast, during the early Holocene, conditions were much wetter with a greening of the Sahara (e.g. Ritchie et al., 1985; Watrin et al., 2009; Claussen et al., 2017) and abundant lakes and rivers due to the higher latitudes attained by the major rainbelt during summer because of increased solar insolation (e.g. Damnati, 2000; deMenocal et al., 2000; Drake et al., 2011; Dupont and Schefuß, 2018; Tierney et al., 2017). This interval is known as the African Humid Period 1 (AHP1) and is clearly expressed by reduced proportions of dust in the sediments of all three studied sites (as indicated by both geochemical ratios (Collins et al., 2013b; Straub et al., 2013) and ^{230}Th-normalised sediment fluxes (Adkins et al., 2006; Bouimetarhan et al., 2012), and also by low deuterium isotopic signatures of plant waxes (Dupont and Schefuß, 2018; Niedermeyer et al., 2010). Pollen reconstructions suggest that vegetation assemblages that developed between 19 and 29°N during AHP1 had no modern analogue, with coexisting savanna and tropical taxa (Hély et al., 2014; Lézine, 2009; Watrin et al., 2009).

The most northerly site, ODP 658 records a trend of decreasing charcoal fluxes as glacial conditions intensified, with charcoal fluxes close to minimum during the LGM (Fig. 5). One possible hypothesis for the observed decrease in charcoal fluxes approaching the LGM is a decrease in wind strength (Kinsley et al., 2022), although at ODP 658, there is no clear trend in dust fluxes which matches the decrease in charcoal fluxes from ca. 50−20 ka. An alternative hypothesis for the decrease in charcoal flux is a reduction in fuel load available to burn attributable to increasing glacial aridity, likely akin to present day locations experiencing less than ca. 800−1000 mm/yr MAP (Archibald and Hempson, 2016; Pausas and Ribeiro, 2013; van der Werf et al., 2008). Biome reconstructions for the LGM suggest that the Saharan Desert expanded southwards to 12°N, displacing the grassy savanna (Collins et al., 2013a; Dupont, 2011; Hoogakker et al., 2016) and reducing both the total biomass of vegetation and the area of land susceptible to burning. The degree of aridity at the LGM is currently debated (e.g. Gasse, 2000; McGee et al., 2013; Niedermeyer et al., 2010; Scheff et al., 2017; Shanahan et al., 2016), however, the increase in ln[Zr/Al] values at ODP 658 towards the LGM supports an aridification trend (Fig. 5).

Following the LGM, there is an increase in charcoal fluxes into the Holocene at ODP 658, a result also seen further north in Morocco (Reddad et al., 2013; Tabel et al., 2016). We interpret this signal to result from a more humid climate (indicated by low δD and ln[Zr/Al] values, Fig. 5) permitting the spread of flammable plant material into previously desert regions. Evidence of a migration of a diverse woody savanna biome into the desert region is provided by increased proportions of Cyperaceae and Poaceae pollen at and around ODP 658 (Dupont, 2011; Dupont and Schefuß, 2018), with a northward shift in the reconstructed Sahara-Sahel boundary position to ~20°N (Collins et al., 2013a), very close to the latitude of ODP 658 (Fig. 8). There is also evidence of increased winter rainfall linked to an intensification and southward shift of Mediterranean storm tracks in the northernmost part of Africa (Blanchet et al., 2021; Cheddadi et al., 2021). Estimates of annual rainfall values around the latitude of ODP 658 range from ca. 350−1200 mm/yr during AHP1 (Larrasoaña et al., 2013; Tierney et al., 2017). Precipitation minus evaporation has been suggested as a more important control on fire activity than absolute precipitation (Daniau et al., 2012), however, distinguishing between these potential drivers is difficult from the existing proxy reconstructions (e.g. Collins et al., 2013b; Govin et al., 2012; Smith and Freeman, 2006; White and Blum, 1995). Increased seasonality of precipitation and/or an increase in ignition frequency due to increased storm activity could also have contributed to elevated fire activities, with increased biomass production during the wet season followed by
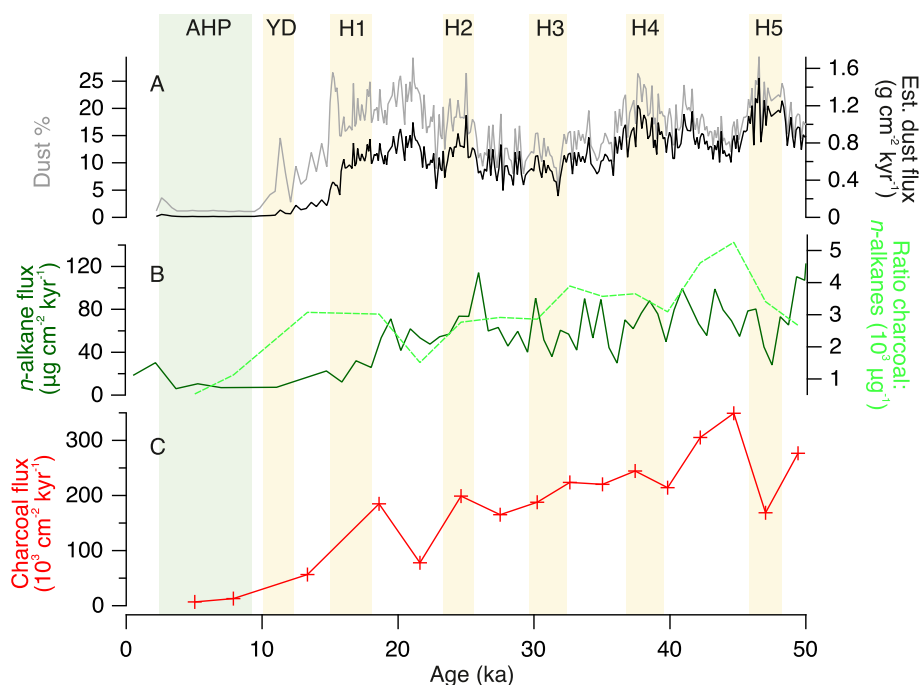
Fig. 5. Hydroclimate reconstructions and charcoal fluxes at the northern end of our transect. Data are from ODP 658 and nearby site GeoB7920-2. a) Hydrogen isotope ratio of C_{31} *n*-alkanes at GeoB7920-2 (20° 45′ N, 18° 35′ W) with error bars of 1 standard deviation plotted (blue, Dupont and Schefuβ, 2018). Lower values are interpreted as representing more humid conditions. b) ln[Zr/Al] values of bulk sediment at ODP 658 obtained by X-ray fluorescence core scanning (light green, Meckler et al., 2013). Dark green line indicates 5-point running mean. High values are interpreted as indicating a high proportion of coarse-grained dust in the sediment. c) Terrigenous (light purple) and dust (dark purple) fluxes to ODP 658C estimated using ^{230}Th-normalisation and grain size distributions, with error bars of 1 standard deviation plotted (Adkins et al., 2006; Kinsley et al., 2022). d) Flux of microscopic charcoal particles to ODP 658 (red, this study). Green vertical bar indicates African Humid Period 1 (AHP1), yellow vertical bars mark approximate ages of stadials associated with Heinrich events 1−5 (HS1-HS5) and the Younger Dryas (YD). (For interpretation of the references to colour in this figure legend, the reader is referred to the Web version of this article.)
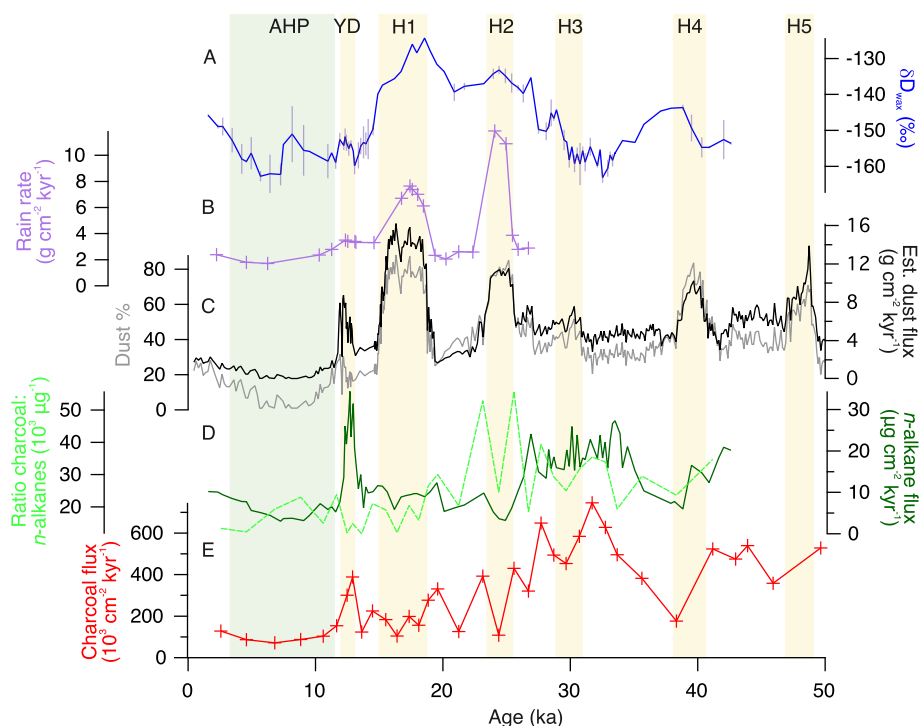
Fig. 6. Hydroclimate reconstructions and plant wax and charcoal fluxes to our central site. All data are from GB-08. a) Hydrogen isotope ratio of C_{31} *n*-alkanes with error bars of 1 standard deviation plotted (blue, Niedermeyer et al., 2010). b) Rain rate (purple) estimated using ^{230}Th-normalisation (Bouimetarhan et al., 2012; Lippold et al., 2012) c) Dust % (as a proportion of the lithogenic fraction) estimated from major element composition (grey, Collins et al., 2013a) . Dust fluxes (black) calculated from dust % values, Ca concentrations (Zabel, 2010), dry bulk densities and sedimentation rates. d) Total flux of $C_{27}−C_{34}$ *n*-alkanes (dark green, Niedermeyer et al., 2010) and ratio of concentrations of charcoal to $C_{27}−C_{34}$ *n*-alkanes (light green). e) Flux of microscopic charcoal particles to GB-08 (red, this study). (For interpretation of the references to colour in this figure legend, the reader is referred to the Web version of this article.)

Fig. 7. Hydroclimate reconstructions and plant wax and charcoal fluxes to our southernmost site. All data are from GB-28. a) Dust % (as a proportion of the lithogenic fraction) estimated from major element composition (grey, Collins et al., 2013a). Dust fluxes (black) estimated from dust % values, Ca concentrations (Collins et al., 2013a), dry bulk densities and sedimentation rates. b) Total flux of $C_{29}-C_{33}$ n-alkanes (dark green, Schreuder et al., 2019) and ratio of concentrations of charcoal to $C_{29}-C_{33}$ n-alkanes (light green). c) Flux of microscopic charcoal particles to GB-28 (red, this study). (For interpretation of the references to colour in this figure legend, the reader is referred to the Web version of this article.)

desiccation during the dry season resulting in large fuel loads (Bond and Keeley, 2005; Gill, 1975). Both data and model-based reconstructions of climate suggest that there may have been increased seasonality of precipitation in the mid-Holocene, but limited data coverage and difficulty in reproducing AHP precipitation in most climate models currently leads to some uncertainty in this result (Brierley et al., 2020; Hély et al., 2014; Hopcroft et al., 2017; Pausata et al., 2016; Perez-Sanz et al., 2014; Peyron et al., 2006).

Fire activity at site GB-28 shows quite different behaviour to ODP 658 (Fig. 7). Higher charcoal fluxes during glacial conditions (50−18 ka) than the Holocene can clearly be seen despite the lower temporal resolution of the data from this site. Similarly high fire activities under glacial conditions have been recorded at low latitude sites RC27-04 in the eastern equatorial Atlantic (Verardo and Ruddiman, 1996), Lake Challa on the Kenya-Tanzania border (Nelson et al., 2012) and Lake Bosumtwi in Ghana (Shanahan et al., 2016). Pollen data from sediment cores close to GB-28 record high grass percentages under glacial conditions, with the total palynological assemblage interpreted as recording a southward expansion of C4 savannas (including grass-rich dry open woodland) and a reduction in tropical rainforest extent (Castañeda et al., 2009; Collins et al., 2011; Dupont and Agwu, 1992; Lézine and Casanova, 1991). Modern savanna ecosystems are characterised by higher fire activities than the tropical rainforests (van der Werf et al., 2008). We suggest that a southwards (relative to modern) expansion of flammable savanna grasslands, likely supported by increased drying of fuel sources under more arid conditions, is responsible for the higher glacial charcoal fluxes at our southernmost site, GB-28. Strengthened glacial winds may have also aided charcoal transport to site GB-28 during the late glacial period (Bradtmiller et al., 2016; McGee et al., 2013), but were unlikely to be the main controlling factor on charcoal fluxes because of the response to peak glacial conditions observed further north (lower

charcoal fluxes than during the Holocene) and elevated charcoal to n-alkane ratios (both of which are likely transported by similar mechanisms) recorded at GB-28 during the glacial period (Fig. 7).

Transitioning into the Holocene, GB-28 shows a striking decline in charcoal fluxes (Fig. 8). This is in contrast to the high fire activities recorded today at this latitude (9°N; Fig. 1) (Archibald et al., 2013; Giglio et al., 2006), with local vegetation consisting of a mosaic of tropical grasslands, shrublands and broadleaf forests (Olson et al., 2001). Modern precipitation values in this region vary from approximately 1000 mm/yr (inland) to >2500 mm/yr (coastal regions), spanning the range associated with a peak burned fraction of vegetation to an environment with very limited burning (Archibald and Hempson, 2016, Fig. 2). Both savanna and forests are stable biomes within this precipitation range, with fire acting to differentiate between the two (Staver et al., 2011b). We therefore suggest that fire activity at these latitudes became suppressed during AHP1 with rainfall likely exceeding the modern threshold above which outright suppression is observed (ca. 1500−2000 mm/yr), or a "too-wet to burn" scenario (Archibald and Hempson, 2016; Staver et al., 2011a; van der Werf et al., 2008). Increased precipitation would have supported a higher proportion of C3 woody plants, as observed in both the pollen and n-alkane $\delta^{13}C$ records (Castañeda et al., 2009; Dupont, 2011). Charcoal flux data to assess mid-versus late Holocene burning are not available, but an increase in the flux of the fire biomarker levoglucosan (Schreuder et al., 2019) suggests that fire activity increased towards modern levels in the late Holocene associated with the termination of the AHP (Supplementary Fig. 2).

Site GB-08, located in between ODP 658 and GB-28, shows a different trend in charcoal fluxes over the past 50 kyr to that shown at either of the other two sites. During the last glacial period, charcoal fluxes decreased towards low values at the LGM, following a similar trend to that documented at ODP 658. We infer a driving mechanism common to both sites, namely the southward
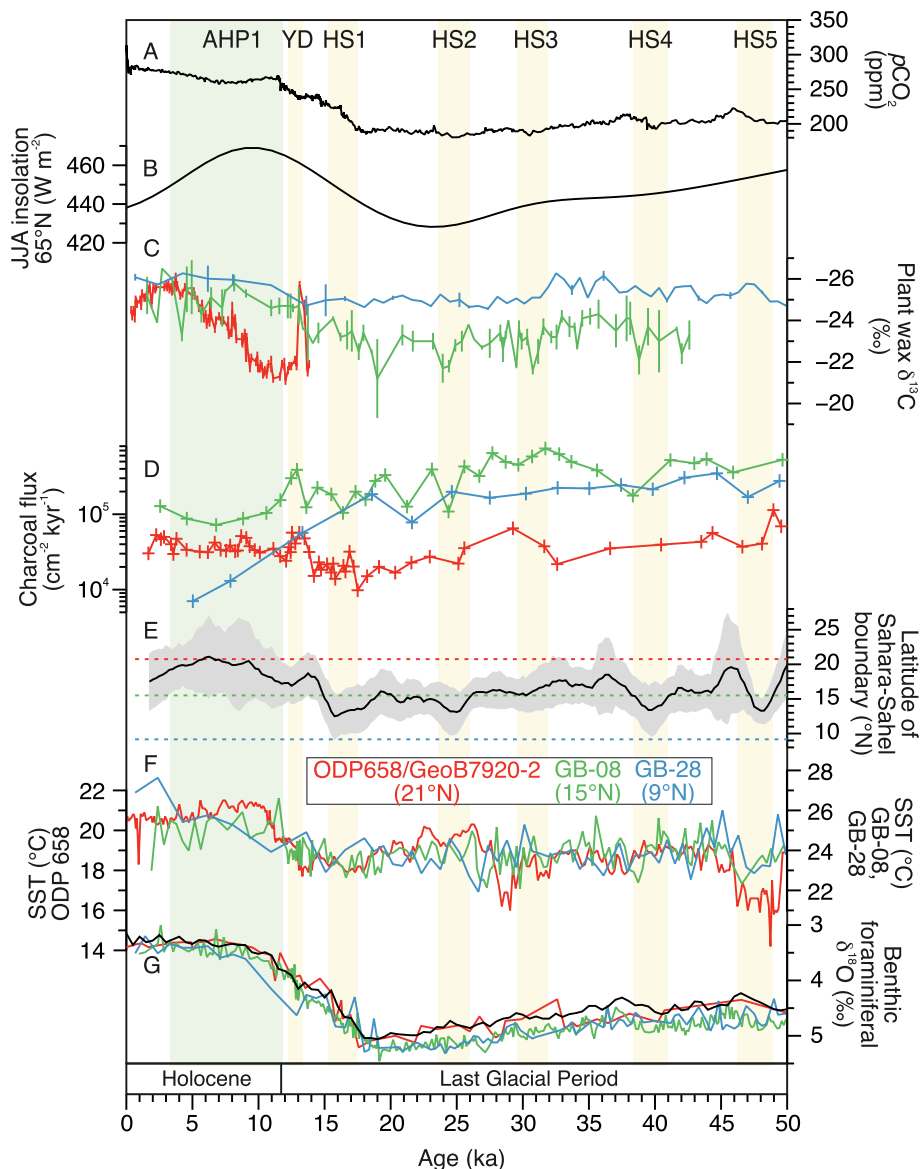
Fig. 8. Comparison of fire and vegetation changes along the Northwest African Margin Transect to global climate records. Data from ODP 658 and nearby site GeoB7920-2 shown in red, GB-08 in green and GB-28 in blue. a) Atmospheric pCO$_2$ from a composite Antarctic ice core record (Bereiter et al., 2015 and references therein). b) Mean boreal summer insolation (June-August) at 65°N given by the La2004 orbital solution (Laskar et al., 2004). c) δ^{13}C signatures of plant waxes (C$_{31}$ n-alkanes) from GeoB7920-2 (red, Dupont and Schefuß, 2018), GB-08 (green, Niedermeyer et al., 2010) and GB-28 (blue, Castañeda et al., 2009). Error bars indicate 1 standard deviation. d) Charcoal flux at ODP 658 (red), GB-08 (green) and GB-28 (blue) (this study). Note logarithmic scale on y-axis. e) Reconstructed latitude of the Sahara-Sahel boundary (five-point running average) based upon major element compositions of marine sediment, with 68% confidence interval plotted (Collins et al., 2013a). Horizontal lines mark the latitudes of ODP 658 (red), GB-08 (green) and GB-28 (blue). f) Sea surface temperature reconstructions from ODP 658 (red, alkenone-derived, Zhao et al., 1995), GB-08 (green, from foraminiferal Mg/Ca, Zarriess et al., 2011), GB-28 (blue, alkenone-derived, Lopes dos Santos et al., 2010). g) Benthic oxygen isotope values from ODP 658 (red, Sarnthein and Tiedemann, 1990), GB-08 (green, Mulitza et al., 2008b), GB-28 (blue, Castañeda et al., 2009) and deep North Atlantic stack (black, Lisiecki and Stern, 2016). Values from the three African margin sites have been adjusted by + 0.64‰ to correct for species-specific offsets from isotopic equilibrium. High δ^{18}O values indicate large global ice volumes and cold bottom water temperature. (For interpretation of the references to colour in this figure legend, the reader is referred to the Web version of this article.)

expansion of desert conditions reducing the fuel loads for burning. This interpretation is supported by low fluxes of plant leaf waxes (n-alkanes) exported to Site GB-08 during the LGM (Niedermeyer et al., 2010).

Moving into the Holocene, the charcoal flux profiles of the two northern sites diverge. At ODP 658, charcoal values are much higher than during the LGM, while fire activity recorded at GB-08 reaches minimal values in the mid Holocene (Fig. 6), as also observed at southern site GB-28. This result suggests that the "too wet to burn" Holocene conditions recorded at GB-28 may have extended north of ~10°N. Reconstructed rainfall values of ~700−1000 mm/yr MAP

at 15°N during AHP1 (Larrasoaña et al., 2013) are close to the threshold at which fire activity becomes suppressed in modern day Africa (Archibald and Hempson, 2016; van der Werf et al., 2008), with values of >1000 mm/yr MAP occurring south of 15°N and possibly also at higher latitudes over shorter lived events (Larrasoaña et al., 2013; Tierney et al., 2017). Incursions of more humid-adapted species from wooded grasslands and tropical forests during AHP1 are evidenced to at least 25°N in pollen reconstructions (Hoelzmann et al., 1998; Watrin et al., 2009), with pollen records indicating an increase in less flammable sedges concordant with more negative n-alkane δ^{13}C values indicating an
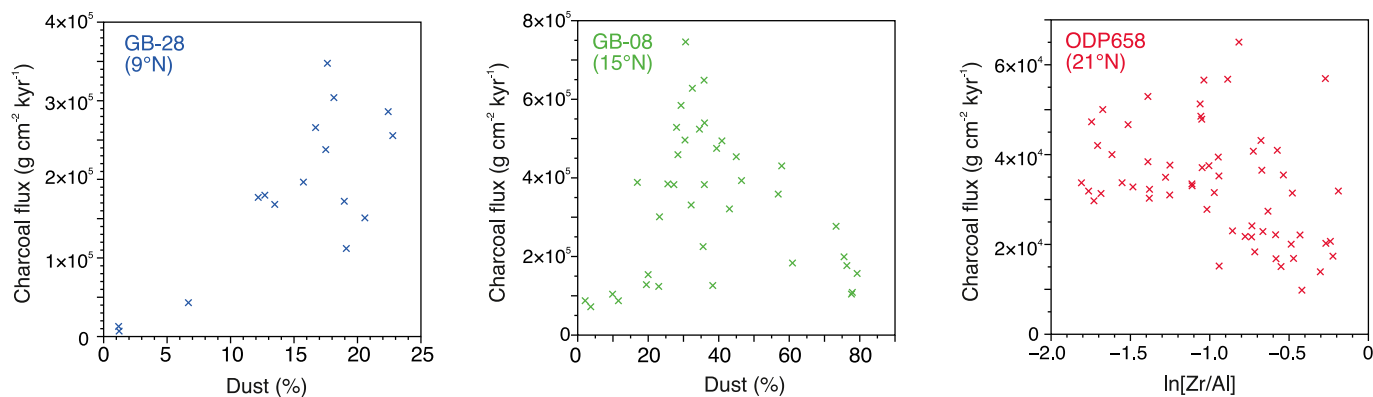
Fig. 9. Cross-plots of charcoal flux (this study) against percentage of total terrigenous content of sediment at GB-28 and GB-08 attributed to dust (left and centre panels) (Collins et al., 2013a) and ln[Zr/Al] values of bulk sediment (a dust proxy) obtained by X-ray fluorescence core scanning at ODP Site 658 (right panel) (Meckler et al., 2013). High ln[Zr/Al] values indicate high dust proportions. We use hydroclimate indices based on geochemical ratios of sediment at all three sites because they are less influenced by wind strength variability than flux reconstructions and continuous, high-resolution records are available at all three sites.

increase in C_3 plants at GB-08, similar to that recorded at GB-28 (Fig. 8, Bouimetarhan et al., 2012; Castañeda et al., 2009; Niedermeyer et al., 2010).

The different trends in charcoal fluxes at each of our three sites highlight the importance of local climate in driving fire activity on North Africa over the past 50 kyr. Recent work has also highlighted the importance of pCO$_2$ on glacial-interglacial biome shifts, particularly the balance between C_3 and C_4 plants, which indirectly impacts fire activity (e.g. Bond et al., 2003; Prentice et al., 2017). Atmospheric carbon dioxide levels of ~180 ppm during the late glacial period would have suppressed tree growth both in wooded savannas and at forest-grassland boundaries by decreasing water use efficiencies and severely slowing woody plant regrowth rates after fires (Bond and Midgley, 2000, 2012; Polley et al., 1997; Prentice et al., 2011; Wooller et al., 2000). The southward expansion of the southern limit of savanna grasslands into previously more wooded biomes, which is proposed to drive a decrease in fire activity through the last deglaciation at the southern end of our transect, may therefore be a result of both increased aridity and low glacial pCO$_2$. Similarly, both fire and low pCO$_2$ are proposed to act to stabilise glacial tropical grasslands in nearby Ghana (Shanahan et al., 2016).

On a global scale, temperature has been identified as the main driver of glacial-interglacial trends in fire activity (Daniau et al., 2012), with elevated Holocene fire activity compared to LGM burning widely documented (Daniau et al., 2010; Marlon et al., 2016; Power et al., 2008). However, the differences in charcoal flux trends at each of our three sites rules out temperature as the main driver of fire activity in Northern Africa over the past 50 kyr. Sea surface temperature reconstructions at all three studied sites show warmer temperatures in the Holocene than the last glacial period (Lopes dos Santos et al., 2010; Zarriess et al., 2011; Zhao et al., 1995, Fig. 8). Continental temperature reconstructions are sparse, but results suggest a similar temperature history across North Africa (e.g. Bartlein et al., 2011; Tierney et al., 2020). Thus, cold glacial temperatures, expected to suppress burning (Daniau et al., 2010), therefore may contribute to the low glacial fire activities at ODP 658. Studies of modern ecosystems suggest that temperature sensitivity of fire is greatest in the most productive ecosystems (Pausas and Ribeiro, 2013), however the high glacial fire activities recorded at low latitude site GB-28 imply that the impact of hydroclimate change and related biome shifts overwhelmed temperature effects on North Africa despite the high primary productivity at these latitudes today (e.g. Running et al., 2000).

3.2.2. Millennial-scale variability

During the last glacial interval, the climate of northern Africa was punctuated by periods of extreme drought associated with cooling of the North Atlantic Ocean during Heinrich (H-)events (e.g. Collins et al., 2013a; Mulitza et al., 2008b; Tjallingii et al., 2008). This cooling led to the Sahara-Sahel boundary shifting ca. 3—4° southwards from its pre-event position (Collins et al., 2013a; Mulitza et al., 2008b), a much greater shift than the estimated global mean southward displacement of the ITCZ position (~0.6°) (McGee et al., 2014). As a result, precipitation over West Africa was reduced, accompanied by a strengthening of the African Easterly Jet (AEJ) (Kinsley et al., 2022; Middleton et al., 2018; Mulitza et al., 2008b).

At our mid-transect site GB-08 (~15°N), lower charcoal fluxes are recorded in the intervals of increased dust input associated with Heinrich events measured in the same sediment core (Fig. 6). However, there appears to be no clear correspondence between charcoal flux minima and Heinrich events at the most northerly (ODP 658) and southerly (GB-28) ends of our transect (21°N and 9°N respectively) (Fig. 8). At the northern end of the transect, HS1 is the only Heinrich stadial clearly expressed in ln[Zr/Al] and shows a small increase in charcoal flux record above Last Glacial Maximum values. Variability in charcoal in the rest of the glacial does not correspond to documented hydroclimate variability in the ln[Zr/Al] record. H-events are also only weakly expressed in the dust record at GB-28, and we find no conclusive evidence for a major fire activity response in the samples taken at these depths (although data resolution is low). We also record a peak in charcoal flux at ca. 13 ka at both ODP 658 and GB-08. These two peaks fall in the later part of the humid interval associated with the warmth of the Bølling-Allerød period (high ln[Zr/Al] and low % dust) and the transition to the drier and more dusty Younger Dryas (Collins et al., 2013a; Meckler et al., 2013).

We attribute the contrasting sensitivity of fire regime and aridity during H-events at each of the three sites to their positions relative to the latitude of the boundary between desert and grasslands. Reconstructions suggest the Sahara-Sahel boundary shifted southwards from approximately 16°N to 13°N during H-events (Collins et al., 2013a; Mulitza et al., 2008b, Fig. 8), with fossil sand dunes identified as far south as 14°N (e.g. Grove, 1958). Under these conditions, site GB-08 at 15°N would be greatly influenced by its proximity to the shift from flammable grassland to fuel-limited desert during H-events, leading to a decline in fire activity. Sites ODP 658 and GB-28, located at 21°N and 9°N, respectively, are situated thousands of kilometers from this major vegetation

boundary migration, where we might expect ecosystem changes and their effects on fire activity to be much less pronounced. Today, vegetation coverage is minimal at 21°N with desert at this latitude, therefore any further intensification of the arid baseline state would not have caused major biomass shifts at the northern end of our latitudinal transect. The comparative insensitivity to H-event climate forcing in the fire regime at the southern end of our transect is consistent with the lack of a signal in plant wax $\delta^{13}C$ to indicate a shift in the relative proportions of C_3 and C_4 plants (Fig. 8, Castañeda et al., 2009).

3.2.3. "Goldilocks" fire activity

Our results reveal a strong latitudinal signal in fire activity response on Africa to changing climate over the last 50 kyrs. We attribute this result to a strongly inflected, 'hump-shaped' relationship between fire activity and rainfall, whereby burning is greatest at intermediate precipitation levels (Fig. 2). Such a relationship is observed in modern African ecosystems, where peak fire activity is documented at intermediate levels of precipitation, with decreasing fire activity outside a range of 800−1400 mm/yr MAP (Archibald and Hempson, 2016; Pausas and Ribeiro, 2013; van der Werf et al., 2008). Our results provide evidence of such a relationship from the palaeo-record over multi-millennial timescales.

At our southernmost site, GB-28, we report low fire activity at times for which humid conditions are reconstructed, and high fire activities at times of aridity (Fig. 7). This positive correlation between fire activity and aridity has also been observed over a range of timescales at other near-equatorial localities such as the Niger Delta (Morley and Richards, 1993), Tropical Atlantic (Verardo and Ruddiman, 1996), Uganda (Colombaroli et al., 2014), Mount Kenya (Rucina et al., 2009), Ghana (Shanahan et al., 2016), and northeast Nigeria, where fire activity is greatest at times of low water levels (Waller et al., 2007). The increase in fire activity at GB-28 during drier intervals such as the LGM suggests that conditions at about 9°N were not dry enough at any point during the last 50 kyr to transition to a situation where fire activity became fuel-limited.

ODP 658, our northernmost site, exhibits the opposite relationship between fire activity and precipitation to GB-28, with increased charcoal fluxes broadly occurring at times of enhanced humidity and very low charcoal fluxes during more arid conditions, as indicated by high ln[Zr/Al] values (Fig. 5). Decreasing fire activity with increasing aridity is recorded in arid/semi-arid regions of Africa over a range of timescales, including southern Algeria (Lécuyer et al., 2016), Mali (Neumann et al., 2009), Morocco (Reddad et al., 2013; Tabel et al., 2016), Lake Malawi (Cohen et al., 2007) and southern Africa (Daniau et al., 2013). In these environments, increased precipitation generally promoted greater biomass production, resulting in a larger fuel stocks and increased fire activity (van der Werf et al., 2008). In contrast, when precipitation levels were similar to today (or lower), such as during the LGM, much of northern Africa became a highly inhospitable environment for all but the most resilient forms of life (Gasse, 2000; Kuechler et al., 2013; Swezey, 2001) and fire activity was supressed by low fuel loads.

GB-08, our mid-transect site, exhibits the most striking relationship between precipitation and fire activity. Here, charcoal fluxes are lowered relative to the late Holocene both during the wettest (AHP1) and driest (H-events) intervals of the last 50 kyr (Fig. 7), resulting in a humped relationship peaking at intermediate aridity. This site is situated close to the latitude of the modern grassy savanna-woody savanna boundary (Fig. 1), and hence is sensitive to the latitudinal shifts in the Sahara-Sahel boundary identified through our studied interval (Fig. 8) (Collins et al., 2013a). Palaeo-precipitation reconstructions estimate MAP values of ca. 1000 mm/yr MAP at 15°N during AHP (Larrasoaña et al., 2013;

Tierney et al., 2017), close to values at which modern fire activities start to decrease with increased precipitation as burning becomes limited by moisture rather than fuel availability (Archibald and Hempson, 2016; van der Werf et al., 2008). A similar sensitivity of fire activity to precipitation is recorded in Lake Naivasha, in currently fuel-limited semi-arid Kenya, where marked variation in forest and woodland plants versus grasses over the past 1200 years shows evidence of fire suppression when climates became sub-humid (Colombaroli et al., 2014). However, records exhibiting this "Goldilocks" behaviour between precipitation and fire activity are rare, and this behaviour has not previously been documented over multi-millennial timescales on Africa.

The highest charcoal fluxes at GB-08 over the last 50 kyr are associated with estimated sediment dust percentages of 25−45% (Fig. 9). Comparable dust percentage values in surface/late Holocene sediments are found approximately 15−20°N (13−22°N at 1σ confidence level) (Collins et al., 2013a), largely to the north of the main band of fire activity today (~9−15°N). This offset between modern and palaeo-fire activity may be a result of anthropogenic impacts modifying the relationship between fire activity, either directly through changing ignition frequency (Bowman et al., 2011; Whitlock et al., 2010) and land-use shifts modifying ecosystems (Gornitz and NASA, 1985) and elevating dust fluxes (Mulitza et al., 2010) or indirectly through regional climate change (e.g. Kgope et al., 2010; Park et al., 2016). Alternatively, past vegetation assemblages without a modern analogue, such as those identified during AHP1 (Hély et al., 2014; Watrin et al., 2009) may have responded differently to climatic forcing. Variability in $p\text{CO}_2$ throughout the last 50 kyr likely also modified the relationship between precipitation and fire activity through its influence on vegetation assemblages and biomass (Bond and Midgley, 2012; Prentice et al., 2011, 2017). An influence of stronger glacial winds (McGee et al., 2013; Skonieczny et al., 2019) driving increases in both charcoal fluxes and dust accumulation is also possible, however transport effects are not a dominant control on charcoal fluxes at these sites over the last 50 kyr (see section 3.1.2).

3.3. Strong imprint of human activity on palaeo fire activity in central and western North Africa unlikely

Human activity can act to both increase or suppress fire through direct impacts such as changing ignition rates and timing, and indirectly through impacts on land use, ecosystem structure and fuel loads (Archibald et al., 2012; Bowman et al., 2011; Whitlock et al., 2010). However, it is generally accepted that an increase in charcoal fluxes is associated with the onset of anthropogenic forcing on fire activity (e.g. Power et al., 2008; Thevenon et al., 2010). Human activity can change the frequency of ignitions but not the fuel load (except through significant land use modification e.g. grazing livestock in grasslands) (Archibald et al., 2012). Major expansion in West African populations and agriculture occurred in the Late Holocene (Manning and Timpson, 2014; Ozainne et al., 2014). The timing of the onset of human-controlled fire activity is debated, with estimates of the timing of humans first developing the ability to create fire ranging from ca. 1900−200 kyr ago (e.g. Bowman et al., 2009; Gowlett, 2006; Wrangham et al., 1999). Regardless, a distinctive human impact on fire regimes in Africa is considered unlikely before 40−4 kyr ago (Archibald et al., 2012). Schreuder et al. (2019) invoke human hunting practices to explain a short-lived increase in the fire biomarker levoglucosan recorded at GB-28 approximately 55 kyr ago. However, the lack of an increase in charcoal fluxes in the youngest (Late Holocene) part of our records and the clear relationship between aridity and fire activity argues against human activity as the key control on our charcoal fluxes (although aridity would have likely also influenced human

activity (e.g. Sereno et al., 2008)). A lack of human control over the reconstructed fire activities is supported by multiple records from East African lakes and the Mediterranean (where early human populations are much better documented than in northwestern Africa and modern fire activities are lower) which suggest that fires triggered by human activity only became dominant over natural events over the last few millennia or even centuries (e.g. Colombaroli et al., 2014; Thevenon et al., 2003; Turner et al., 2008), in agreement with global trends (Marlon et al., 2008). We therefore consider a major anthropogenic impact on fire activity at our sites unlikely before the use of fire for large-scale land clearance and agropastoralism ca. 4000 years ago (Archibald et al., 2012).

4. Conclusions

We report strong latitudinal variation in the response of fire activity to rainfall climate shifts over the last 50 kyr based on new records of charcoal flux to three marine sediment cores along the northwest African margin. At our most northerly site (ODP 658, 21°N), fire activity is highest during more humid intervals of desert greening such as AHP1, while our most southerly site (GB-28, 9°N) shows the opposite response, with peak burning at times of aridity (e.g. the last glacial period). We attribute these different responses in fire activity between the two sites to different mechanisms limiting fire activity at each end of the rainfall gradient. At ODP 658, insolation-driven increases in rainfall promoted the expansion of flammable grassy savanna into desert regions, increasing both fuel load and dry-season ignition events. In contrast, increased precipitation at southern site GB-28 increased the proportion of woody plants at the expense of more flammable grass biomass and increased fuel moisture content, suppressing fire activity. Our mid-transect site (GB-08, 15°N) lies in the latitudinal band of the modern Sahel and exhibits reduced burning relative to today during both the wettest (e.g. AHP1) and driest (e.g. H1−4) intervals of the last 50 kyrs, with maxima in fire activity occurring at intermediate humidity levels. GB-08 is located closest to the Sahara-Sahel boundary, which shifted both northwards and southwards of the site over the last 50 kyr, resulting in major biome shifts as a response to both astronomically-paced insolation forcing and millennial-scale re-organisation of ocean circulation and North Atlantic surface ocean temperatures. When comparing the fire activity-dust relationship across the last 50 kyr with that observed today, peak charcoal fluxes over the last 50 kyr are associated with higher dust concentrations in marine sediments (implying more arid conditions) than found today adjacent to the highest fire activities. This difference may result from anthropogenic impacts on burning today, the influence of changing pCO_2 and/or non-analogue past ecosystems responding differently to climatic forcing. Our records suggest that, in contrast to the global picture, precipitation is the dominant driver of changes in fire activity on Africa over the last 50 kyrs through its control over vegetation assemblages and flammability, resulting in major latitudinal variability in the temporal evolution of biomass burning.

Data availability

Datasets related to this article are available as supplementary files and also on the open access database Zenodo (https://doi.org/10.5281/zenodo.6554310).

Author contribution statement

Harriet R. Moore: Methodology, Investigation, Writing − original draft, Visualization.; **Anya J. Crocker:** Conceptualization, Data curation, Writing − original draft, Writing − review & editing,

Visualization, Supervision.; **Claire M. Belcher:** Conceptualization, Methodology, Writing − review & editing.; **A. Nele Meckler:** Writing − review & editing.; **Colin Osborne:** Conceptualization, Writing − review & editing.; **David Beerling:** Conceptualization, Writing − review & editing, Funding acquisition.; **Paul Wilson:** Conceptualization, Writing − original draft, Writing − review & editing, Supervision, Funding acquisition.

Declaration of competing interest

The authors declare that they have no known competing financial interests or personal relationships that could have appeared to influence the work reported in this paper.

Appendix A. Supplementary data

Supplementary data to this article can be found online at https://doi.org/10.1016/j.quascirev.2022.107578.

References

Accatino, F., De Michele, C., Vezzoli, R., Donzelli, D., Scholes, R.J., 2010. Tree−grass co-existence in savanna: interactions of rain and fire. J. Theor. Biol. 267, 235−242.

Adkins, J., deMenocal, P., Eshel, G., 2006. The "African humid period" and the record of marine upwelling from excess 230Th in Ocean Drilling Program Hole 658C. Paleoceanography 21, PA4203.

Archibald, S., 2016. Managing the Human Component of Fire Regimes: Lessons from Africa, vol. 371. Philosophical Transactions of the Royal Society B: Biological Sciences.

Archibald, S., Hempson, G.P., 2016. Competing Consumers: Contrasting the Patterns and Impacts of Fire and Mammalian Herbivory in Africa, vol. 371. Philosophical Transactions of the Royal Society B: Biological Sciences.

Archibald, S., Lehmann, C.E.R., Belcher, C.M., Bond, W.J., Bradstock, R.A., Daniau, A.L., Dexter, K.G., Forrestel, E.J., Greve, M., He, T., Higgins, S.I., Hoffmann, W.A., Lamont, B.B., McGlinn, D.J., Moncrieff, G.R., Osborne, C.P., Pausas, J.G., Price, O., Ripley, B.S., Rogers, B.M., Schwilk, D.W., Simon, M.F., Turetsky, M.R., van der Werf, G.R., Zanne, A.E., 2018. Biological and geophysical feedbacks with fire in the Earth system. Environ. Res. Lett. 13, 033003.

Archibald, S., Lehmann, C.E.R., Gómez-Dans, J.L., Bradstock, R.A., 2013. Defining pyromes and global syndromes of fire regimes. Proc. Natl. Acad. Sci. Unit. States Am. 110, 6442−6447.

Archibald, S., Roy, D.P., Van Wilgen, B.W., Scholes, R.J., 2009. What limits fire? An examination of drivers of burnt area in Southern Africa. Global Change Biol. 15, 613−630.

Archibald, S., Staver, A.C., Levin, S.A., 2012. Evolution of human-driven fire regimes in Africa. Proc. Natl. Acad. Sci. Unit. States Am. 109, 847−852.

Bartlein, P.J., Harrison, S.P., Brewer, S., Connor, S., Davis, B.A.S., Gajewski, K., Guiot, J., Harrison-Prentice, T.I., Henderson, A., Peyron, O., Prentice, I.C., Scholze, M., Seppä, H., Shuman, B., Sugita, S., Thompson, R.S., Viau, A.E., Williams, J., Wu, H., 2011. Pollen-based continental climate reconstructions at 6 and 21 ka: a global synthesis. Clim. Dynam. 37, 775−802.

Beckage, B., Platt, William J., Gross, Louis J., 2009. Vegetation, fire, and feedbacks: a disturbance-mediated model of savannas. Am. Nat. 174, 805−818.

Beerling, D.J., Osborne, C.P., 2006. The origin of the savanna biome. Global Change Biol. 12, 2023−2031.

Bereiter, B., Eggleston, S., Schmitt, J., Nehrbass-Ahles, C., Stocker, T.F., Fischer, H., Kipfstuhl, S., Chappellaz, J., 2015. Revision of the EPICA Dome C CO2 record from 800 to 600 kyr before present. Geophys. Res. Lett. 42, 542−549.

Bird, M.I., Cali, J.A., 1998. A million-year record of fire in sub-Saharan Africa. Nature 394, 767−769.

Bird, M.I., Moyo, C., Veenendaal, E.M., Lloyd, J., Frost, P., 1999. Stability of elemental carbon in a savanna soil. Global Biogeochem. Cycles 13, 923−932.

Blaauw, M., Christen, J.A., 2011. Flexible paleoclimate age-depth models using an autoregressive gamma process. Bayesian Anal. 6, 457−474.

Blanchet, C.L., Osborne, A.H., Tjallingii, R., Ehrmann, W., Friedrich, T., Timmermann, A., Brückmann, W., Frank, M., 2021. Drivers of river reactivation in North Africa during the last glacial cycle. Nat. Geosci. 14 (2), 97−103.

Bond, W.J., Keeley, J.E., 2005. Fire as a global 'herbivore': the ecology and evolution of flammable ecosystems. Trends Ecol. Evol. 20, 387−394.

Bond, W.J., Midgley, G.F., 2000. A proposed CO2-controlled mechanism of woody plant invasion in grasslands and savannas. Global Change Biol. 6, 865−869.

Bond, W.J., Midgley, G.F., 2012. Carbon dioxide and the uneasy interactions of trees and savannah grasses. Phil. Trans. Biol. Sci. 367, 601−612.

Bond, W.J., Midgley, G.F., Woodward, F.I., 2003. The importance of low atmospheric CO2 and fire in promoting the spread of grasslands and savannas. Global Change Biol. 9, 973−982.

Bond, W.J., Woodward, F.I., Midgley, G.F., 2005. The global distribution of ecosystems in a world without fire. New Phytol. 165, 525−538.

Bouimetarhan, I., Prange, M., Schefuß, E., Dupont, L., Lippold, J., Mulitza, S., Zonneveld, K., 2012. Sahel megadrought during Heinrich Stadial 1: evidence for a three-phase evolution of the low- and mid-level West African wind system. Quat. Sci. Rev. 58, 66−76.

Bowman, D.M.J.S., Balch, J., Artaxo, P., Bond, W.J., Cochrane, M.A., D'Antonio, C.M., DeFries, R., Johnston, F.H., Keeley, J.E., Krawchuk, M.A., Kull, C.A., Mack, M., Moritz, M.A., Pyne, S., Roos, C.I., Scott, A.C., Sodhi, N.S., Swetnam, T.W., 2011. The human dimension of fire regimes on Earth. J. Biogeogr. 38, 2223−2236.

Bowman, D.M.J.S., Balch, J.K., Artaxo, P., Bond, W.J., Carlson, J.M., Cochrane, M.A., D'Antonio, C.M., DeFries, R.S., Doyle, J.C., Harrison, S.P., Johnston, F.H., Keeley, J.E., Krawchuk, M.A., Kull, C.A., Marston, J.B., Moritz, M.A., Prentice, I.C., Roos, C.I., Scott, A.C., Swetnam, T.W., van der Werf, G.R., Pyne, S.J., 2009. Fire in the Earth system. Science 324, 481−484.

Bowman, D.M.J.S., Murphy, B.P., Williamson, G.J., Cochrane, M.A., 2014. Pyrogeographic models, feedbacks and the future of global fire regimes. Global Ecol. Biogeogr. 23, 821−824.

Bradtmiller, L.I., McGee, D., Awalt, M., Evers, J., Yerxa, H., Kinsley, C.W., deMenocal, P., 2016. Changes in biological productivity along the northwest African margin over the past 20,000 years. Paleoceanography 31, 185−202.

Brierley, C.M., Zhao, A., Harrison, S.P., Braconnot, P., Williams, C.J.R., Thornalley, D.J.R., Shi, X., Peterschmitt, J.Y., Ohgaito, R., Kaufman, D.S., Kageyama, M., Hargreaves, J.C., Erb, M.P., Emile-Geay, J., D'Agostino, R., Chandan, D., Carré, M., Bartlein, P.J., Zheng, W., Zhang, Z., Zhang, Q., Yang, H., Volodin, E.M., Tomas, R.A., Routson, C., Peltier, W.R., Otto-Bliesner, B., Morozova, P.A., McKay, N.P., Lohmann, G., Legrande, A.N., Guo, C., Cao, J., Brady, E., Annan, J.D., Abe-Ouchi, A., 2020. Large-scale features and evaluation of the PMIP4-CMIP6 midHolocene simulations. Clim. Past 16, 1847−1872.

Cardoso, A.W., Oliveras, I., Abernethy, K.A., Jeffery, K.J., Lehmann, D., Edzang Ndong, J., McGregor, I., Belcher, C.M., Bond, W.J., Malhi, Y.S., 2018. Grass species flammability, not biomass, drives changes in fire behavior at tropical forest-savanna transitions. Front. For. Glob. Change 1.

Castañeda, I.S., Mulitza, S., Schefuß, E., Lopes dos Santos, R.A., Sinninghe Damsté, J.S., Schouten, S., 2009. Wet phases in the Sahara/Sahel region and human migration patterns in North Africa. Proc. Natl. Acad. Sci. Unit. States Am. 106, 20159−20163.

Cheddadi, R., Carré, M., Nourelbait, M., François, L., Rhoujjati, A., Manay, R., Ochoa, D., Schefuß, E., 2021. Early Holocene greening of the Sahara requires Mediterranean winter rainfall. Proc. Natl. Acad. Sci. Unit. States Am. 118, e2024898118.

Clark, J.S., 1988. Particle motion and the theory of charcoal analysis: source area, transport, deposition, and sampling. Quat. Res. 30, 67−80.

Clarke, H., Penman, T., Boer, M., Cary, G.J., Fontaine, J.B., Price, O., Bradstock, R., 2020. The proximal drivers of large fires: a pyrogeographic study. Front. Earth Sci. 8.

Claussen, Martin, Dallmeyer, Anne, Claussen, Jürgen, 2017. Theory and modeling of the African humid period and the green Sahara. Oxford Research Encyclopedia of Climate Science. Oxford University Press.

Cohen, A.S., Stone, J.R., Beuning, K.R.M., Park, L.E., Reinthal, P.N., Dettman, D., Scholz, C.A., Johnson, T.C., King, J.W., Talbot, M.R., Brown, E.T., Ivory, S.J., 2007. Ecological consequences of early Late Pleistocene megadroughts in tropical Africa. Proc. Natl. Acad. Sci. Unit. States Am. 104, 16422−16427.

Collins, J.A., Govin, A., Mulitza, S., Heslop, D., Zabel, M., Hartmann, J., Roehl, U., Wefer, G., 2013a. Abrupt shifts of the Sahara-Sahel boundary during Heinrich stadials. Clim. Past 9, 1181−1191.

Collins, J.A., Schefuß, E., Heslop, D., Mulitza, S., Prange, M., Zabel, M., Tjallingii, R., Dokken, T.M., Huang, E., Mackensen, A., Schulz, M., Tian, J., Zarriess, M., Wefer, G., 2011. Interhemispheric symmetry of the tropical African rainbelt over the past 23,000 years. Nat. Geosci. 4, 42−45.

Collins, J.A., Schefuß, E., Mulitza, S., Prange, M., Werner, M., Tharammal, T., Paul, A.,

Wefer, G., 2013b. Estimating the hydrogen isotopic composition of past precipitation using leaf-waxes from western Africa. Quat. Sci. Rev. 65, 88−101.

Colombaroli, D., Ssemmanda, I., Gelorini, V., Verschuren, D., 2014. Contrasting long-term records of biomass burning in wet and dry savannas of equatorial East Africa. Global Change Biol. 20, 2903−2914.

D'Onofrio, D., von Hardenberg, J., Baudena, M., 2018. Not only trees: grasses determine African tropical biome distributions via water limitation and fire. Global Ecol. Biogeogr. 27, 714−725.

Damnati, B., 2000. Holocene lake records in the northern hemisphere of Africa. J. Afr. Earth Sci. 31, 253−262.

Daniau, A.-L., Bartlein, P.J., Harrison, S.P., Prentice, I.C., Brewer, S., Friedlingstein, P., Harrison-Prentice, T.I., Inoue, J., Izumi, K., Marlon, J.R., Mooney, S., Power, M.J., Stevenson, J., Tinner, W., Andrič, M., Atanassova, J., Behling, H., Black, M., Blarquez, O., Brown, K.J., Carcaillet, C., Colhoun, E.A., Colombaroli, D., Davis, B.A.S., D'Costa, D., Dodson, J., Dupont, L., Eshetu, Z., Gavin, D.G., Genries, A., Haberle, S., Hallett, D.J., Hope, G., Horn, S.P., Kassa, T.G., Katamura, F., Kennedy, L.M., Kershaw, P., Krivonogov, S., Long, C., Magri, D., Marinova, E., McKenzie, G.M., Moreno, P.I., Moss, P., Neumann, F.H., Norström, E., Paitre, C., Rius, D., Roberts, N., Robinson, G.S., Sasaki, N., Scott, L., Takahara, H., Terwilliger, V., Thevenon, F., Turner, R., Valsecchi, V.G., Vannière, B., Walsh, M., Williams, N., Zhang, Y., 2012. Predictability of biomass burning in response to climate changes. Global Biogeochem. Cycles 26.

Daniau, A.-L., Sánchez Goñi, M.F., Martinez, P., Urrego, D.H., Bout-Roumazeilles, V., Desprat, S., Marlon, J.R., 2013. Orbital-scale climate forcing of grassland burning in southern Africa. Proc. Natl. Acad. Sci. Unit. States Am. 110, 5069−5073.

Daniau, A.L., Harrison, S.P., Bartlein, P.J., 2010. Fire regimes during the last glacial. Quat. Sci. Rev. 29, 2918−2930.

deMenocal, P., Ortiz, J., Guilderson, T., Adkins, J., Sarnthein, M., Baker, L., Yarusinsky, M., 2000. Abrupt onset and termination of the African Humid Period: rapid climate responses to gradual insolation forcing. Quat. Sci. Rev. 19, 347−361.

deMenocal, P.B., 1995. Plio-pleistocene African climate. Science 270, 53−59.

Drake, N.A., Blench, R.M., Armitage, S.J., Bristow, C.S., White, K.H., 2011. Ancient watercourses and biogeography of the Sahara explain the peopling of the desert. Proc. Natl. Acad. Sci. Unit. States Am. 108, 458−462.

Dupont, L., 2011. Orbital scale vegetation change in Africa. Quat. Sci. Rev. 30, 3589−3602.

Dupont, L.M., 1993. Vegetation zones in NW Africa during the brunhes chron reconstructed from marine palynological data. Quat. Sci. Rev. 12, 189−202.

Dupont, L.M., Agwu, C.O.C., 1992. Latitudinal shifts of forest and savanna in N. W. Africa during the Brunhes chron: further marine palynological results from site M 16415 (9°N 19°W). Veg. Hist. Archaeobotany 1, 163−175.

Dupont, L.M., Schefuß, E., 2018. The roles of fire in Holocene ecosystem changes of West Africa. Earth Planet Sci. Lett. 481, 255−263.

Eldrett, J.S., Harding, I.C., Firth, J.V., Roberts, A.P., 2004. Magnetostratigraphic calibration of Eocene−Oligocene dinoflagellate cyst biostratigraphy from the Norwegian−Greenland Sea. Mar. Geol. 204, 91−127.

Gasse, F., 2000. Hydrological changes in the African tropics since the last glacial Maximum. Quat. Sci. Rev. 19, 189−211.

Giglio, L., van der Werf, G.R., Randerson, J.T., Collatz, G.J., Kasibhatla, P., 2006. Global estimation of burned area using MODIS active fire observations. Atmos. Chem. Phys. 6, 957−974.

Gill, A.M., 1975. Fire and the Australian Flora: a review. Aust. For. 38, 4−25.

Goldberg, E.D., 1985. Black Carbon in the Environment: Properties and Distribution. J. Wiley, New York.

Gornitz, V., NASA, 1985. A survey of anthropogenic vegetation changes in West Africa during the last century — climatic implications. Climatic Change 7, 285−325.

Govin, A., Holzwarth, U., Heslop, D., Ford Keeling, L., Zabel, M., Mulitza, S., Collins, J.A., Chiessi, C.M., 2012. Distribution of major elements in Atlantic surface sediments (36°N−49°S): imprint of terrigenous input and continental weathering. G-cubed 13, Q01013.

Gowlett, J.A.J., 2006. The early settlement of northern Europe: fire history in the context of climate change and the social brain. Comptes Rendus Palevol 5, 299−310.

Grousset, F.E., Parra, M., Bory, A., Martinez, P., Bertrand, P., Shimmield, G., Ellam, R.M., 1998. Saharan wind regimes traced by the Sr−Nd isotopic composition of subtropical Atlantic sediments: last Glacial Maximum vs today. Quat. Sci. Rev. 17, 395−409.

Grove, A.T., 1958. The ancient Erg of Hausaland, and similar formations on the south side of the Sahara. Geogr. J. 124, 528−533.

Hély, C., Lézine, A.M., APD contributors, 2014. Holocene changes in African vegetation: tradeoff between climate and water availability. Clim. Past 10, 681−686.

Herring, J.R., 1985. Charcoal Fluxes into Sediments of the North Pacific Ocean: the Cenozoic Record of Burning, the Carbon Cycle and Atmospheric CO2: Natural Variations Archean to Present. American Geophysical Union, pp. 419−442.

Higuera, P.E., Whitlock, C., Gage, J.A., 2011. Linking tree-ring and sediment-charcoal records to reconstruct fire occurrence and area burned in subalpine forests of Yellowstone National Park, USA. Holocene 21, 327−341.

Hoelzmann, P., Jolly, D., Harrison, S.P., Laarif, F., Bonnefille, R., Pachur, H.-J., 1998. Mid-Holocene land-surface conditions in northern Africa and the Arabian Peninsula: a data set for the analysis of biogeophysical feedbacks in the climate system. Global Biogeochem. Cycles 12, 35−51.

Hoetzel, S., Dupont, L., Schefuß, E., Rommerskirchen, F., Wefer, G., 2013. The role of fire in Miocene to Pliocene C4 grassland and ecosystem evolution. Nat. Geosci.

6, 1027−1030.

Hoffmann, W.A., Geiger, E.L., Gotsch, S.G., Rossatto, D.R., Silva, L.C.R., Lau, O.L., Haridasan, M., Franco, A.C., 2012. Ecological thresholds at the savanna-forest boundary: how plant traits, resources and fire govern the distribution of tropical biomes. Ecol. Lett. 15, 759−768.

Hoogakker, B.A.A., Smith, R.S., Singarayer, J.S., Marchant, R., Prentice, I.C., Allen, J.R.M., Anderson, R.S., Bhagwat, S.A., Behling, H., Borisova, O., Bush, M., Correa-Metrio, A., de Vernal, A., Finch, J.M., Fréchette, B., Lozano-Garcia, S., Gosling, W.D., Granoszewski, W., Grimm, E.C., Grüger, E., Hanselman, J., Harrison, S.P., Hill, T.R., Huntley, B., Jiménez-Moreno, G., Kershaw, P., Ledru, M.P., Magri, D., McKenzie, M., Müller, U., Nakagawa, T., Novenko, E., Penny, D., Sadori, L., Scott, L., Stevenson, J., Valdes, P.J., Vandergoes, M., Velichko, A., Whitlock, C., Tzedakis, C., 2016. Terrestrial biosphere changes over the last 120 kyr. Clim. Past 12, 51−73.

Hooghiemstra, H., Agwu, C.O.C., 1986. Distribution of palynomorphs in marine sediments: a record for seasonal wind patterns over NW Africa and adjacent Atlantic. Geol. Rundsch. 75, 81−95.

Hooghiemstra, H., Lézine, A.-M., Leroy, S.A.G., Dupont, L., Marret, F., 2006. Late Quaternary palynology in marine sediments: a synthesis of the understanding of pollen distribution patterns in the NW African setting. Quat. Int. 148, 29−44.

Hopcroft, P.O., Valdes, P.J., Harper, A.B., Beerling, D.J., 2017. Multi vegetation model evaluation of the Green Sahara climate regime. Geophys. Res. Lett. 44, 6804−6813.

Keeley, J.E., Rundel, P.W., 2005. Fire and the Miocene expansion of C4 grasslands. Ecol. Lett. 8, 683−690.

Kgope, B.S., Bond, W.J., Midgley, G.F., 2010. Growth responses of African savanna trees implicate atmospheric [CO2] as a driver of past and current changes in savanna tree cover. Austral Ecol. 35, 451−463.

Kinsley, C.W., Bradtmiller, L.I., McGee, D., Galgay, M., Stuut, J.-B., Tjallingii, R., Winckler, G., deMenocal, P.B., 2022. Orbital- and millennial-scale variability in northwest African dust emissions over the past 67,000 years. Paleoceanogr. Paleoclimatol. 36, e2020PA004137.

Krastel, S., Hanebuth, T.J.J., Antobreh, A.A., Henrich, R., Holz, C., Kölling, M., Schulz, H.D., Wien, K., Wynn, R.B., 2004. CapTimiris Canyon: a newly discovered channel system offshore of Mauritania. Eos, Trans. Am. Geophys. Union 85, 417−423.

Krawchuk, M.A., Moritz, M.A., Parisien, M.-A., Van Dorn, J., Hayhoe, K., 2009. Global pyrogeography: the current and future distribution of wildfire. PLoS One 4, e5102.

Kuechler, R.R., Schefuß, E., Beckmann, B., Dupont, L., Wefer, G., 2013. NW African hydrology and vegetation during the Last Glacial cycle reflected in plant-wax-specific hydrogen and carbon isotopes. Quat. Sci. Rev. 82, 56−67.

Larrasoaña, J.C., Roberts, A.P., Rohling, E.J., 2013. Dynamics of green Sahara periods and their role in hominin evolution. PLoS One 8, e76514.

Laskar, J., Robutel, P., Joutel, F., Gastineau, M., Correia, A.C.M., Levrard, B., 2004. A long-term numerical solution for the insolation quantities of the Earth. Astron. Astrophys. 428, 261−285.

Lécuyer, C., Lézine, A.-M., Fourel, F., Gasse, F., Sylvestre, F., Pailles, C., Grenier, C., Travi, Y., Barral, A., 2016. I-n-Atei paleolake documents past environmental changes in central Sahara at the time of the "Green Sahara": charcoal, carbon isotope and diatom records. Palaeogeogr. Palaeoclimatol. Palaeoecol. 441, 834−844.

Lézine, A.-M., 2009. Timing of vegetation changes at the end of the Holocene Humid Period in desert areas at the northern edge of the Atlantic and Indian monsoon systems. Compt. Rendus Geosci. 341, 750−759.

Lézine, A.-M., Casanova, J., 1991. Correlated oceanic and continental records demonstrate past climate and hydrology of North Africa (0-140 ka). Geology 19, 307−310.

Lippold, J., Mulitza, S., Mollenhauer, G., Weyer, S., Heslop, D., Christl, M., 2012. Boundary scavenging at the East Atlantic margin does not negate use of 231Pa/230Th to trace Atlantic overturning. Earth Planet Sci. Lett. 333−334, 317−331.

Lisiecki, L.E., Raymo, M.E., 2005. A Pliocene-Pleistocene stack of 57 globally distributed benthic δ18O records. Paleoceanography 20.

Lisiecki, L.E., Stern, J.V., 2016. Regional and global benthic δ18O stacks for the last glacial cycle. Paleoceanography 31, 1368−1394.

Lopes dos Santos, R.A., Prange, M., Castañeda, I.S., Schefuß, E., Mulitza, S., Schulz, M., Niedermeyer, E.M., Sinninghe Damsté, J.S., Schouten, S., 2010. Glacial−interglacial variability in Atlantic meridional overturning circulation and thermocline adjustments in the tropical North Atlantic. Earth Planet Sci. Lett. 300, 407−414.

Manning, K., Timpson, A., 2014. The demographic response to Holocene climate change in the Sahara. Quat. Sci. Rev. 101, 28−35.

Marlon, J.R., Bartlein, P.J., Carcaillet, C., Gavin, D.G., Harrison, S.P., Higuera, P.E., Joos, F., Power, M.J., Prentice, I.C., 2008. Climate and human influences on global biomass burning over the past two millennia. Nat. Geosci. 1, 697−702.

Marlon, J.R., Kelly, R., Daniau, A.L., Vannière, B., Power, M.J., Bartlein, P., Higuera, P., Blarquez, O., Brewer, S., Brücker, T., Feurdean, A., Romera, G.G., Iglesias, V., Maezumi, S.Y., Magi, B., Courtney Mustaphi, C.J., Zhihai, T., 2016. Reconstructions of biomass burning from sediment-charcoal records to improve data−model comparisons. Biogeosciences 13, 3225−3244.

Masiello, C.A., 2004. New directions in black carbon organic geochemistry. Mar. Chem. 92, 201−213.

McGee, D., deMenocal, P.B., Winckler, G., Stuut, J.B.W., Bradtmiller, L.I., 2013. The magnitude, timing and abruptness of changes in North African dust deposition over the last 20,000 yr. Earth Planet Sci. Lett. 371−372, 163−176.

McGee, D., Donohoe, A., Marshall, J., Ferreira, D., 2014. Changes in ITCZ location and cross-equatorial heat transport at the last glacial Maximum, Heinrich stadial 1, and the mid-holocene. Earth Planet Sci. Lett. 390, 69−79.

Meckler, A.N., Sigman, D.M., Gibson, K.A., Francois, R., Martinez-Garcia, A., Jaccard, S.L., Rohl, U., Peterson, L.C., Tiedemann, R., Haug, G.H., 2013. Deglacial pulses of deep-ocean silicate into the subtropical North Atlantic Ocean. Nature 495, 495−498.

Middleton, J.L., Mukhopadhyay, S., Langmuir, C.H., McManus, J.F., Huybers, P.J., 2018. Millennial-scale variations in dustiness recorded in Mid-Atlantic sediments from 0 to 70 ka. Earth Planet Sci. Lett. 482, 12−22.

Morley, R.J., Richards, K., 1993. Gramineae cuticle: a key indicator of Late Cenozoic climatic change in the Niger Delta. Rev. Palaeobot. Palynol. 77, 119−127.

Mulitza, S., Heslop, D., Pittauerova, D., Fischer, H.W., Meyer, I., Stuut, J.-B., Zabel, M., Mollenhauer, G., Collins, J.A., Kuhnert, H., Schulz, M., 2010. Increase in African dust flux at the onset of commercial agriculture in the Sahel region. Nature 466, 226−228.

Mulitza, S., Krastel, S., Wefer, G., 2008a. Climate history and sedimentation processes off NW Africa - cruise No. M65 - june 11 - august 10, 2005 - Dakar (Senegal) - Las palmas (Spain). In: DFG-Senatskommission für Ozeanographie. METEOR-Berichte, Bremen, pp. 1−114.

Mulitza, S., Prange, M., Stuut, J.-B., Zabel, M., von Dobeneck, T., Itambi, A.C., Nizou, J., Schulz, M., Wefer, G., 2008b. Sahel megadroughts triggered by glacial slowdowns of Atlantic meridional overturning. Paleoceanography 23, PA4206.

Nelson, D.M., Verschuren, D., Urban, M.A., Hu, F.S., 2012. Long-term variability and rainfall control of savanna fire regimes in equatorial East Africa. Global Change Biol. 18, 3160−3170.

Neumann, K., Fahmy, A., Lespez, L., Ballouche, A., Huysecom, E., 2009. The early Holocene palaeoenvironment of Ounjougou (Mali): phytoliths in a multiproxy context. Palaeogeogr. Palaeoclimatol. Palaeoecol. 276, 87−106.

Nicholson, S., 2009. A revised picture of the structure of the "monsoon" and land ITCZ over West Africa. Clim. Dynam. 32, 1155−1171.

Nicholson, S.E., Grist, J.P., 2003. The seasonal evolution of the atmospheric circulation over West Africa and equatorial Africa. J. Clim. 16, 1013−1030.

Niedermeyer, E.M., Schefuß, E., Sessions, A.L., Mulitza, S., Mollenhauer, G., Schulz, M., Wefer, G., 2010. Orbital- and millennial-scale changes in the hydrologic cycle and vegetation in the western African Sahel: insights from individual plant wax δD and δ13C. Quat. Sci. Rev. 29, 2996−3005.

Olson, D.M., Dinerstein, E., Wikramanayake, E.D., Burgess, N.D., Powell, G.V.N., Underwood, E.C., D'Amico, J.A., Itoua, I., Strand, H.E., Morrison, J.C., Loucks, C.J., Allnutt, T.F., Ricketts, T.H., Kura, Y., Lamoreux, J.F., Wettengel, W.W., Hedao, P., Kassem, K.R., 2001. Terrestrial ecoregions of the world: a new map of life on Earth. Bioscience 51, 933−938.

Osborne, C.P., Beerling, D.J., 2006. Nature's green revolution: the remarkable evolutionary rise of C4 plants. Phil. Trans. Biol. Sci. 361, 173−194.

Ozainne, S., Lespez, L., Garnier, A., Ballouche, A., Neumann, K., Pays, O., Huysecom, E., 2014. A question of timing: spatio-temporal structure and mechanisms of early agriculture expansion in West Africa. J. Archaeol. Sci. 50, 359−368.

Paillard, D., Labeyrie, L., Yiou, P., 1996. Macintosh Program performs time-series analysis. Eos, Trans. Am. Geophys. Union 77, 379-379.

Park, J.-y., Bader, J., Matei, D., 2016. Anthropogenic Mediterranean warming essential driver for present and future Sahel rainfall. Nat. Clim. Change 6, 941−945.

Pausas, J.G., Keeley, J.E., Schwilk, D.W., 2017. Flammability as an ecological and evolutionary driver. J. Ecol. 105, 289−297.

Pausas, J.G., Ribeiro, E., 2013. The global fire−productivity relationship. Global Ecol. Biogeogr. 22, 728−736.

Pausata, F.S.R., Messori, G., Zhang, Q., 2016. Impacts of dust reduction on the northward expansion of the African monsoon during the Green Sahara period. Earth Planet Sci. Lett. 434, 298−307.

Perez-Sanz, A., Li, G., González-Sampériz, P., Harrison, S.P., 2014. Evaluation of modern and mid-Holocene seasonal precipitation of the Mediterranean and northern Africa in the CMIP5 simulations. Clim. Past 10, 551−568.

Peyron, O., Jolly, D., Braconnot, P., Bonnefille, R., Guiot, J., Wirrmann, D., Chalié, F., 2006. Quantitative reconstructions of annual rainfall in Africa 6000 years ago: model-data comparison. J. Geophys. Res. Atmos. 111.

Polley, H.W., Mayeux, H.S., Johnson, H.B., Tischler, C.R., 1997. Viewpoint: atmospheric CO2, soil water, and shrub/grass ratios on rangelands. J. Range Manag. 50, 278−284.

Power, M.J., Marlon, J., Ortiz, N., Bartlein, P.J., Harrison, S.P., Mayle, F.E., Ballouche, A., Bradshaw, R.H.W., Carcaillet, C., Cordova, C., Mooney, S., Moreno, P.I., Prentice, I.C., Thonicke, K., Tinner, W., Whitlock, C., Zhang, Y., Zhao, Y., Ali, A.A., Anderson, R.S., Beer, R., Behling, H., Briles, C., Brown, K.J., Brunelle, A., Bush, M., Camill, P., Chu, G.Q., Clark, J., Colombaroli, D., Connor, S., Daniau, A.L., Daniels, M., Dodson, J., Doughty, E., Edwards, M.E., Finsinger, W., Foster, D., Frechette, J., Gaillard, M.J., Gavin, D.G., Gobet, E., Haberle, S., Hallett, D.J., Higuera, P., Hope, G., Horn, S., Inoue, J., Kaltenrieder, P., Kennedy, L., Kong, Z.C., Larsen, C., Long, C.J., Lynch, J., Lynch, E.A., McGlone, M., Meeks, S., Mensing, S., Meyer, G., Minckley, T., Mohr, J., Nelson, D.M., New, J., Newnham, R., Noti, R., Oswald, W., Pierce, J., Richard, P.J.H., Rowe, C., Sanchez Goñi, M.F., Shuman, B.N., Takahara, H., Toney, J., Turney, C., Urrego-Sanchez, D.H., Umbanhowar, C., Vandergoes, M., Vanniere, B., Vescovi, E., Walsh, M., Wang, X., Williams, N., Wilmshurst, J., Zhang, J.H., 2008. Changes in fire regimes since the Last Glacial Maximum: an assessment based on a global synthesis and analysis of charcoal data. Clim. Dynam. 30, 887−907.

Prell, W.L., Kutzbach, J.E., 1987. Monsoon variability over the past 150,000 years. J. Geophys. Res. Atmos. 92, 8411–8425.

Prentice, I.C., Cleator, S.F., Huang, Y.H., Harrison, S.P., Roulstone, I., 2017. Reconstructing ice-age palaeoclimates: quantifying low-CO2 effects on plants. Global Planet. Change 149, 166–176.

Prentice, I.C., Harrison, S.P., Bartlein, P.J., 2011. Global vegetation and terrestrial carbon cycle changes after the last ice age. New Phytol. 189, 988–998.

Reddad, H., Etabaai, I., Rhoujjati, A., Taieb, M., Thevenon, F., Damnati, B., 2013. Fire activity in North West Africa during the last 30,000 cal years BP inferred from a charcoal record from Lake Ifrah (Middle atlas–Morocco): climatic implications. J. Afr. Earth Sci. 84, 47–53.

Ripley, B., Donald, G., Osborne, C.P., Abraham, T., Martin, T., 2010. Experimental investigation of fire ecology in the C3 and C4 subspecies of Alloteropsis semialata. J. Ecol. 98, 1196–1203.

Ritchie, J.C., Eyles, C.H., Haynes, C.V., 1985. Sediment and pollen evidence for an early to mid-Holocene humid period in the eastern Sahara. Nature 314, 352.

Rucina, S.M., Muiruri, V.M., Kinyanjui, R.N., McGuiness, K., Marchant, R., 2009. Late Quaternary vegetation and fire dynamics on Mount Kenya. Palaeogeogr. Palaeoclimatol. Palaeoecol. 283, 1–14.

Ruddiman, W.F., Sarnthein, M., Baldauf, J.G., et al., 1989. Proc. ODP, Init. Repts., vol. 108. Ocean Drilling Program), College Station, TX.

Running, S.W., Thornton, P.E., Nemani, R., Glassy, J.M., 2000. Global terrestrial gross and net primary productivity from the Earth observing system. In: Sala, O.E., Jackson, R.B., Mooney, H.A., Howarth, R.W. (Eds.), Methods in Ecosystem Science. Springer New York, New York, NY, pp. 44–57.

Sankaran, M., Hanan, N.P., Scholes, R.J., Ratnam, J., Augustine, D.J., Cade, B.S., Gignoux, J., Higgins, S.I., Le Roux, X., Ludwig, F., Ardo, J., Banyikwa, F., Bronn, A., Bucini, G., Caylor, K.K., Coughenour, M.B., Diouf, A., Ekaya, W., Feral, C.J., February, E.C., Frost, P.G.H., Hiernaux, P., Hrabar, H., Metzger, K.L., Prins, H.H.T., Ringrose, S., Sea, W., Tews, J., Worden, J., Zambatis, N., 2005. Determinants of woody cover in African savannas. Nature 438, 846.

Sarnthein, M., Tiedemann, R., 1990. Younger dryas-style cooling events at glacial terminations I-VI at ODP site 658: associated benthic δ13C anomalies constrain meltwater hypothesis. Paleoceanography 5, 1041–1055.

Scheff, J., Seager, R., Liu, H., Coats, S., 2017. Are glacials dry? Consequences for paleoclimatology and for greenhouse warming. J. Clim. 30, 6593–6609.

Schreuder, L.T., Hopmans, E.C., Castañeda, I.S., Schefuß, E., Mulitza, S., Sinninghe Damsté, J.S., Schouten, S., 2019. Late quaternary biomass burning in northwest Africa and interactions with climate, vegetation, and humans. Paleoceanogr. Paleoclimatol. 34, 153–163.

Sereno, P.C., Garcea, E.A.A., Jousse, H., Stojanowski, C.M., Saliège, J.-F., Maga, A., Ide, O.A., Knudson, K.J., Mercuri, A.M., Stafford Jr., T.W., Kaye, T.G., Giraudi, C., N'Siala, I.M., Cocca, E., Moots, H.M., Dutheil, D.B., Stivers, J.P., 2008. Lakeside cemeteries in the Sahara: 5000 Years of Holocene population and environmental change. PLoS One 3, e2995.

Shackleton, N.J., Fairbanks, R.G., Chiu, T., Parrenin, F., 2004. Absolute calibration of the Greenland time scale: implications for Antarctic time scales and for Δ14C. Quat. Sci. Rev. 23, 1513–1522.

Shanahan, T.M., Hughen, K.A., McKay, N.P., Overpeck, J.T., Scholz, C.A., Gosling, W.D., Miller, C.S., Peck, J.A., King, J.W., Heil, C.W., 2016. CO2 and fire influence tropical ecosystem stability in response to climate change. Sci. Rep. 6, 29587.

Simpson, K.J., Ripley, B.S., Christin, P.-A., Belcher, C.M., Lehmann, C.E.R., Thomas, G.H., Osborne, C.P., 2016. Determinants of flammability in savanna grass species. J. Ecol. 104, 138–148.

Skonieczny, C., McGee, D., Winckler, G., Bory, A., Bradtmiller, L.I., Kinsley, C.W., Polissar, P.J., De Pol-Holz, R., Rossignol, L., Malaizé, B., 2019. Monsoon-driven Saharan dust variability over the past 240,000 years. Sci. Adv. 5, eaav1887.

Skonieczny, C., Paillou, P., Bory, A., Bayon, G., Biscara, L., Crosta, X., Eynaud, F., Malaize, B., Revel, M., Aleman, N., Barusseau, J.P., Vernet, R., Lopez, S., Grousset, F., 2015. African humid periods triggered the reactivation of a large river system in Western Sahara. Nat. Commun. 6.

Smith, F.A., Freeman, K.H., 2006. Influence of physiology and climate on δD of leaf wax n-alkanes from C3 and C4 grasses. Geochem. Cosmochim. Acta 70, 1172–1187.

Staver, A.C., Archibald, S., Levin, S., 2011a. Tree cover in sub-Saharan Africa: rainfall and fire constrain forest and savanna as alternative stable states. Ecology 92, 1063–1072.

Staver, A.C., Archibald, S., Levin, S.A., 2011b. The global extent and determinants of savanna and forest as alternative biome states. Science 334, 230–232.

Stockmarr, J., 1971. Tablets with Spores Used in Absolute Pollen Analysis.

Straub, M., Sigman, D.M., Ren, H., Martínez-García, A., Meckler, A.N., Hain, M.P., Haug, G.H., 2013. Changes in North Atlantic nitrogen fixation controlled by ocean circulation. Nature 501, 200–203.

Swezey, C., 2001. Eolian sediment responses to late Quaternary climate changes: temporal and spatial patterns in the Sahara. Palaeogeogr. Palaeoclimatol. Palaeoecol. 167, 119–155.

Tabel, J., Khater, C., Rhoujjati, A., Dezileau, L., Bouimetarhan, I., Carre, M., Vidal, L., Benkaddour, A., Nourelbait, M., Cheddadi, R., 2016. Environmental changes over the past 25 000 years in the southern Middle Atlas, Morocco. J. Quat. Sci. 31, 93–102.

Thevenon, F., Williamson, D., Bard, E., Anselmetti, F.S., Beaufort, L., Cachier, H., 2010. Combining charcoal and elemental black carbon analysis in sedimentary archives: implications for past fire regimes, the pyrogenic carbon cycle, and the human–climate interactions. Global Planet. Change 72, 381–389.

Thevenon, F., Williamson, D., Vincens, A., Taieb, M., Merdaci, O., Decobert, M., Buchet, G., 2003. A late-Holocene charcoal record from Lake Masoko, SW Tanzania: climatic and anthropologic implications. Holocene 13, 785–792.

Tiedemann, R., Sarnthein, M., Shackleton, N.J., 1994. Astronomic timescale for the pliocene Atlantic δ18O and dust flux records of ocean drilling Program site 659. Paleoceanography 9, 619–638.

Tierney, J.E., Pausata, F.S.R., deMenocal, P.B., 2017. Rainfall regimes of the green Sahara. Sci. Adv. 3, e1601503.

Tierney, J.E., Zhu, J., King, J., Malevich, S.B., Hakim, G.J., Poulsen, C.J., 2020. Glacial cooling and climate sensitivity revisited. Nature 584, 569–573.

Tjallingii, R., Claussen, M., Stuut, J.-B.W., Fohlmeister, J., Jahn, A., Bickert, T., Lamy, F., Rohl, U., 2008. Coherent high- and low-latitude control of the northwest African hydrological balance. Nat. Geosci. 1, 670–675.

Turner, R., Roberts, N., Jones, M.D., 2008. Climatic pacing of Mediterranean fire histories from lake sedimentary microcharcoal. Global Planet. Change 63, 317–324.

van der Werf, G.R., Randerson, J.T., Giglio, L., Collatz, G.J., Kasibhatla, P.S., Arellano Jr., A.F., 2006. Interannual variability in global biomass burning emissions from 1997 to 2004. Atmos. Chem. Phys. 6, 3423–3441.

van der Werf, G.R., Randerson, J.T., Giglio, L., Gobron, N., Dolman, A.J., 2008. Climate controls on the variability of fires in the tropics and subtropics. Global Biogeochem. Cycles 22.

Verardo, D.J., Ruddiman, W.F., 1996. Late Pleistocene charcoal in tropical Atlantic deep-sea sediments: climatic and geochemical significance. Geology 24, 855–857.

Waelbroeck, C., Lougheed, B.C., Vazquez Riveiros, N., Missiaen, L., Pedro, J., Dokken, T., Hajdas, I., Wacker, L., Abbott, P., Dumoulin, J.-P., Thil, F., Eynaud, F., Rossignol, L., Fersi, W., Albuquerque, A.L., Arz, H., Austin, W.E.N., Came, R., Carlson, A.E., Collins, J.A., Dennielou, B., Desprat, S., Dickson, A., Elliot, M., Farmer, C., Giraudeau, J., Gottschalk, J., Henderiks, J., Hughen, K., Jung, S., Knutz, P., Lebreiro, S., Lund, D.C., Lynch-Stieglitz, J., Malaizé, B., Marchitto, T., Martínez-Méndez, G., Mollenhauer, G., Naughton, F., Nave, S., Nürnberg, D., Oppo, D., Peck, V., Peeters, F.J.C., Penaud, A., Portilho-Ramos, R.d.C., Repschläger, J., Roberts, J., Rühlemann, C., Salgueiro, E., Sanchez Goni, M.F., Schönfeld, J., Scussolini, P., Skinner, L.C., Skonieczny, C., Thornalley, D., Toucanne, S., Rooij, D.V., Vidal, L., Voelker, A.H.L., Wary, M., Weldeab, S., Ziegler, M., 2019. Consistently dated Atlantic sediment cores over the last 40 thousand years. Sci. Data 6, 165.

Waller, M.P., Street-Perrott, F.A., Wang, H., 2007. Holocene vegetation history of the Sahel: pollen, sedimentological and geochemical data from Jikariya Lake, north-eastern Nigeria. J. Biogeogr. 34, 1575–1590.

Watrin, J., Lézine, A.-M., Hély, C., 2009. Plant migration and plant communities at the time of the "green Sahara". Compt. Rendus Geosci. 341, 656–670.

White, A.F., Blum, A.E., 1995. Effects of climate on chemical_ weathering in water-sheds. Geochem. Cosmochim. Acta 59, 1729–1747.

White, F., 1983. The Vegetation of Africa, vol. 20. Natural Resources Research, UNESCO, p. 356.

Whitlock, C., Higuera, P.E., McWethy, D.B., Briles, C.E., 2010. Paleoecological perspectives on fire ecology: revisiting the fire-regime concept. Open Ecol. J. 3.

Wooller, M.J., Street-Perrott, F.A., Agnew, A.D.Q., 2000. Late Quaternary fires and grassland palaeoecology of Mount Kenya, East Africa: evidence from charred grass cuticles in lake sediments. Palaeogeogr. Palaeoclimatol. Palaeoecol. 164, 207–230.

Wrangham, Richard W., Jones, James H., Laden, G., Pilbeam, D., Conklin-Brittain, N., 1999. The raw and the stolen: cooking and the ecology of human origins. Curr. Anthropol. 40, 567–594.

Yan, Y.Y., 2005. Intertropical convergence zone (ITCZ). In: Oliver, J.E. (Ed.), Encyclopedia of World Climatology. Springer Netherlands, Dordrecht, pp. 429–432.

Yu, H., Tan, Q., Chin, M., Remer, L.A., Kahn, R.A., Bian, H., Kim, D., Zhang, Z., Yuan, T., Omar, A.H., Winker, D.M., Levy, R.C., Kalashnikova, O., Crepeau, L., Capelle, V., Chédin, A., 2019. Estimates of African dust deposition along the trans-Atlantic transit using the decadelong record of aerosol measurements from CALIOP, MODIS, MISR, and IASI. J. Geophys. Res. Atmos. 124, 7975–7996.

Zabel, M., 2010. Geochemistry of sediment core GeoB9508-5 from the Senegal river mouth. In: MARUM - Center for Marine Environmental Sciences. PANGAEA. U.B.

Zarriess, M., Johnstone, H., Prange, M., Steph, S., Groeneveld, J., Mulitza, S., Mackensen, A., 2011. Bipolar seesaw in the northeastern tropical Atlantic during Heinrich stadials. Geophys. Res. Lett. 38.

Zhao, M., Beveridge, N.A.S., Shackleton, N.J., Sarnthein, M., Eglinton, G., 1995. Molecular stratigraphy of cores off northwest Africa: sea surface temperature history over the last 80 Ka. Paleoceanography 10, 661–675.